SANDIA REPORT

SAND2003-3869
Unlimited Release
Printed October-2003

Self-Assembly of Polymers in Confined Geometries

John G. Curro, John D. McCoy and Yuan Ye

Prepared by
Sandia National Laboratories
Albuquerque, New Mexico 87185 and Livermore, California 94550

Sandia is a multiprogram laboratory operated by Sandia Corporation,
a Lockheed Martin Company, for the United States Department of Energy's
National Nuclear Security Administration under Contract DE-AC04-94AL85000.

Issued by Sandia National Laboratories, operated for the United States Department of Energy by Sandia Corporation.

Available to DOE and DOE contractors from
U.S. Department of Energy
Office of Scientific and Technical Information
P.O. Box 62
Oak Ridge, TN 37831

Telephone: (865)576-8401
Facsimile: (865)576-5728
E-Mail: reports@adonis.osti.gov
Online ordering: http://www.doe.gov/bridge

Available to the public from
U.S. Department of Commerce
National Technical Information Service
5285 Port Royal Rd
Springfield, VA 22161

Telephone: (800)553-6847
Facsimile: (703)605-6900
E-Mail: orders@ntis.fedworld.gov
Online order: http://www.ntis.gov/help/ordermethods.asp?loc=7-4-0#online

SAND2003-3869
Unlimited Release
Printed October 2003

Final Report: LDRD Project 34692
Self-Assembly of Polymers in Confined Geometries

John D. McCoy and Yuan Ye

Department of Materials and Metallurgical Engineering

New Mexico Institute of Mining & Technology

Socorro, NM 87801

John G. Curro

Materials & Process Modeling & Computation Dept.

Sandia National Laboratories

P. O. Box 5800

Albuquerque, NM 87185

Table of Contents

Part 1: Athermal Systems

Abstract

Athermal, tethered chains are modeled with Density Functional (DFT) theory for both the explicit solvent and continuum solvent cases. The structure of DFT is shown to reduce to Self-Consistent-Field (SCF) theory in the incompressible limit where there is symmetry between solvent and monomer, and to Single-Chain-Mean-Field (SCMF) theory in the continuum solvent limit. We show that by careful selection of the reference and ideal systems in DFT theory, self-consistent numerical solutions can be obtained, thereby avoiding the single chain Monte Carlo simulation in SCMF theory. On long length scales, excellent agreement is seen between the simplified DFT theory and Molecular Dynamics simulations of both continuum solvents and explicit-molecule solvents. In order to describe the structure of the polymer and solvent near the surface it is necessary to include compressibility effects and the nonlocality of the field.

1. Introduction

Polymer chains tethered to a surface provide solutions to a number of technologically important problems. Such applications include the synthesis of biocompatible materials, control of protein adsorption, stabilization of colloids, and the modification of surfaces to control hydrophobicity. These are applications where the chains are in the presence of solvents, or "wet-brushes". The "dry-brush", or solvent-less, case is most applicable as a controlled adhesive. Moreover, wet-brushes are commonly analyzed in the dried state with, for instance, atomic force microscopy (AFM). Consequently, it is useful to understand not only the structure of the wet and of the dry brush states individually, but also the relationship between the two.

The purpose of the present investigation is to develop a theory to model the equilibrium structure and properties of tethered polymer layers in the vicinity of the surface. This problem has been studied extensively by many workers in the past. Scaling approaches, where the polymer profile is assumed to be a step function, were developed by Alexander[1] and de Gennes[2]. Self-consistent field (SCF) theories were developed and numerically implemented by a number of workers[3-8]. Milner and collaborators[9] were able to obtain an analytical solution to the SCF problem under certain conditions that leads to a parabolic density profile for the polymer. A related approach, the single chain mean field (SCMF) theory, was developed by Carignano and Szleifer[10] in a manner that, in effect, incorporates a single chain Monte Carlo simulation as part of a self-consistent field theory. The reader is referred to several reviews on tethered polymer chains that have appeared in the recent literature[11-13]. Computer simulations of tethered chains by

Grest and Murat[14-18] and by Lai and Binder[19] have provided valuable insights and made it possible to evaluate the accuracy of the various theories.

Unlike the previous work on this problem, here we develop the theory using classical density functional theory (DFT). Classical DFT approaches the problem of classical particles in an anisotropic environment from a more general perspective than does SCF. Density functional theory was first applied to molecular liquids by Chandler, McCoy, and Singer[20] and subsequently applied to free polymers near surfaces[21-24]. It is worthwhile to reformulate the tethered chain problem within the context of DFT not only because of the theory's generality, but also because doing so illuminates the various approximations that are necessary to recover conventional SCF theories.

We will, first, apply DFT theory to the case of tethered polymer chains in a continuum solvent, a problem studied extensively both by Murat and Grest[15-18] and by Lai and Binder[19] with MD simulation. Carignano and Szleifer[10] obtained excellent agreement with the Murat and Grest simulations with their SCMF theory. As will be shown later, in the appropriate limit our DFT theory gives comparable results to the SCMF approach. However, in our implementation of DFT we are able to obtain solutions numerically, thereby avoiding a Monte Carlo simulation.

Second, we apply our DFT approach to the problem of tethered chains in the presence of an explicit solvent and compare with corresponding MD simulations[17]. To our knowledge, this is the first time quantitative comparisons have been made between theory and simulation for this problem. This application serves to highlight a significant advantage of our DFT approach which is that it points the way toward making improvements in SCF theory.

In this paper we present the details of the DFT application to tethered chains in Appendices A and B. In the theory section we discuss the approximations necessary to make contact with SCF and SCMF theories. We also demonstrate that the theory can be implemented in a manner that allows us to obtain numerical solutions. Later we show results comparing our DFT theory with MD simulations, both in continuum and explicit solvents.

2. Theory

Since both SCF[1-9] and DFT[20-24] theories are, generically, self-consistent-field theories, the specific approximations which distinguish the meaning of the term "SCF theory" from the broader "DFT theory" are largely determined by colloquial usage in the literature. The two approximations that usually distinguish SCF theory are as follows. First, the only explicit length scale in the problem is assumed to be the radius of gyration. This means that all interactions between sites are "local" (i.e., delta functions), and that the chains are "Gaussian Threads" which can be described by a differential equation. Second, the only effect of the repulsive part of the inter-molecular interactions is assumed to be the enforcement of incompressibility. Consequently, incompressibility is constrained in SCF through an undetermined multiplier and repulsive (or excluded volume) interactions are subsequently ignored. As a result, for the tethered chain problem, the only parameters in the SCF calculation are the chain length, N; the Flory-Huggins χ-parameter; and the surface coverage, σ_A. One expects that such calculations would be accurate on long length scales, but would fail to capture short range, local

packing effects. In the current study, we make some, but not all, of the approximations of SCF theory.

The solution method for the density profile of the tethered chains is essentially that of reference 21. The total site density, $\rho(z)$, at a distance z from the wall can be computed from the coupled functional equations

$$\rho(z) = F[U^0(z)]$$
$$U^0(z) = G[\rho(z)] \qquad (2.1)$$

where $U^0(z)$ is an external field whose purpose is to mimic the effects of the solvent and of the other chains on a given tethered chain. The specific development of the forms of these relationships from a free energy functional is detailed in the appendices.

A. *The Ideal and Reference Systems*

The definition and careful manipulation of the ideal system are central to the successful application of DFT to polymeric systems. The importance of the ideal system is clearly shown in the first of Eqs. (2.1) which represents the computation of the density profile of a single tethered chain (i.e., the ideal system) in an external field $U^0(z)$: this is the subject of appendix A. The term "ideal chain" in DFT theory refers to a polymer chain that does not interact explicitly with the other chains in the system. However, depending on the specific choice of the ideal chain, it may or may not interact with itself via, for example, excluded volume interactions. Even though SCF and DFT theories reduce the many chain problem to the considerably simpler, single ideal chain problem, this simpler problem still cannot be solved in closed form in the presence of an external field. Since a freely-jointed-chain, or random walk model, is Markovian, we can calculate

the density distribution in the external field for this model numerically, for example by using the Fourier transform technique described in appendix A. By contrast, in the SCMF theory of Szleifer and coworkers[10] on tethered chains, and in our earlier work on free chains[22,23], the ideal chain problem was solved with intra-molecular excluded volume interactions between chain segments. In order to compute the density distribution for this self-avoiding walk (SAW) model, these workers required Monte Carlo techniques as part of their self-consistent field calculation. In both ideal chain models, the two equations in Eq. 2.1 are solved iteratively until a self-consistent density profile and external field are obtained. Later in this paper we will demonstrate that equivalent results can be obtained from either the random walk or SAW model as the choice for the ideal system.

In order to see the importance of the ideal system more clearly, let us consider the problem of interest in more detail – that is, tethered polymer chains whose segments are a distance z from the tethering surface. The external field $U^0(z) = G[\rho(z)]$ acts on a single tethered chain, the ideal chain, in order to mimic the effects of the other chains in the system in a mean field sense. The form of this field can be found by minimizing the grand potential free energy with respect to the inhomogeneous density profile $\rho(z)$. The algebraic details of this procedure are reviewed in appendix B and leads to Eq. (B.11) that can be rearranged as follows for the polymer and solvent fields

$$U_p^0(r) = U_p(r) - c_{p,s} * \rho_s(r) + \left[\left(\omega^{-1} - \omega_0^{-1}\right) - \rho_{p,ref} c_{p,p}\right] * \frac{\rho_p(r)}{\rho_{p,ref}} \qquad (2.2)$$

$$U_s^0(r) = U_s(r) - c_{s,s} * \rho_s(r) - c_{s,p} * \rho_p(r)$$

where $c_{i,j}(r)$ is the intermolecular direct correlation function between sites of type p (polymer) or s (solvent). The quantity $\omega^{-1}(r)$ is the functional inverse of the intra-molecular correlation function of the fully interacting polymer chains, and $\omega_0^{-1}(r)$ is the

corresponding inverse for the ideal chain. The direct correlation functions in Eq. (2.2) are to be evaluated in the homogeneous reference state of density $\rho_{p,ref}$. In Eq. (2.2), "*" denotes the convolution integral $f * g(r) = \int f(r - r')g(r')\,dr'$. The function U(r) is the bare external field on the fully interacting, inhomogeneous system due to the presence of the surface; the difference $\Delta\rho(r)$ is $\rho(r)-\rho_{ref}$ and $\rho(r)$ is the density profile of the inhomogeneous system. In Eq. (2.2), constant terms in $U^0(r)$ have been dropped since the density profile is sensitive only to differences in the external field. On the other hand, the free energy does depend upon constant offsets in the potentials, and some care must be taken when treating phase transitions where the value of the free energy (and not only the location of its minimum) is of importance[22].

Two choices need to be made at this point for the "ideal" and "reference" systems. The ideal system can be chosen to be either a random walk or a self-avoiding, random walk (SAW) chain. Since the random walk model can be treated numerically, whereas a SAW model requires a simulation, the choice of a random walk model as the ideal system is highly desirable. Whether or not this is a suitable choice is closely tied to the second choice that must be made: that of the reference system.

The reference system is the homogeneous state about which the Helmholtz Free Energy of the inhomogeneous system is expanded in equation (B.6). Commonly, the bulk liquid in equilibrium with the inhomogeneous system is selected as the reference state. This is a reasonable choice for systems such as un-tethered chains in a pore that are clearly in equilibrium with a bulk liquid reservoir. It is important to recognize, however, that the choice of the reference state is arbitrary to a degree. In the case of chains tethered to a surface, the system far from the wall (which the tethered chains are in equilibrium

with) consists of pure solvent: a problematic choice for the reference system. In particular, the division by $\rho_{p,ref}$ in Eqn. (2.2) makes the bracketed term diverge when $\rho_{p,ref}=0$ unless, of course, $\rho(r)=\rho^0(r)$. Consequently, for this choice of reference system, a SAW ideal chain is required for the accurate portrayal of the single chain structure factor of a dilute solution of a polymer in a good solvent in order to avoid the divergence of the field in Eq.(2.2). This was the approach taken in the SCMF theory.

Rather than taking the reference system to be the far-field, polymer density, which is zero, we instead choose the $\rho_{p,ref}$ to be the average density within the polymer layer. It is physically reasonable that the density in the region where the polymer is actually present should determine the physics of the system. This can be achieved by using a "mass weighted" average of the density defined as

$$\rho_{p,ref} = \langle\rho\rangle = \frac{\int_0^H \rho^2(z)dz}{\int_0^H \rho(z)dz} \qquad (2.5)$$

which is appropriate for the one dimensional density profile and field assumed in this work. Note that the "number weighted" average would be zero due to the large volume of solvent far from the surface. For this reference system, $\rho_{p,ref}$ is no longer zero and the bracketed term in Eqn. (2.2) is not dominated by $\left(\rho^{-1}\rho\rho_0^{-1}\right)$ but is controlled by the c(r) term. For sufficiently high surface coverages, ρ_A, such that $\langle\rho\rangle$ is larger than a particular threshold density, ρ^*, our reference system corresponds to a uniform polymer solution in the concentrated or semidilute regime. This crossover density from dilute to semidilute solutions is defined by

$$\rho^* \sigma^3 \sim \frac{3N\sigma^3}{4\pi R_g^3} \sim \frac{3.5}{N^{3\nu-1}} \qquad (2.6)$$

where $R_g \approx N^{\nu}/\sqrt{6}$ and ν is the Flory exponent. Hence, a reasonable choice for the ideal chain consistent with this reference system would be random walk chain with no excluded volume (ν=1/2).

As we proceed to still lower surface coverages, the theory is affected by a second threshold density, the crossover surface coverage, Γ_A^*, from the brush to the "mushroom" regime where the tethered chains no longer overlap with each other

$$\Gamma_A^* \sigma^2 = \frac{\sigma^2}{\pi R_g^2} = \frac{6}{\pi} N^{-2\nu} \qquad (2.7)$$

As long as $\Gamma_A > \Gamma_A^*$ we expect our assumption of a one-dimensional field and profile to be valid. However it is possible that $\langle \rho \rangle < \rho^*$ while $\Gamma_A > \Gamma_A^*$. When this occurs, we take our reference system to be $\rho_{p,ref} = \rho^*$. Since our reference system is still in the semidilute regime, we can still choose our ideal system to be a random walk chain. At surface coverages below Γ_A^* the tethered chains become isolated, and the tethered layer can no longer be described by a one-dimensional field. In this regime, it would be necessary to treat the fields and profiles in a two dimensional generalization of the theory, in a manner similar to the approach of Balazs and coworkers[25].

Thus, it can be seen that our choice of reference system such that $\rho_{p,ref} \geq \rho^*$ allows us to take our ideal chain to be a random walk model. Consequently the term $\left(\rho^{\nu-1} - \rho_0^{\nu-1}\right)$ can be safely ignored and the bracketed term in Eq. (2.2) is essentially

controlled by the direct correlation function $c_{pp}(r)$. This choice of the reference and ideal systems is very beneficial from a computational standpoint since the density profile calculation in Eq. (2.1) can be performed without resorting to a simulation.

B. The Connection Between SCF and DFT Theories

At this point, various simplifying approximations in the spirit of SCF theory can be made. First, the length scale associated with c(r) is assumed to be negligible, and c(r) is treated as a delta function: $c(r) = \hat{c}(0)\delta(r)$. For our choice of ideal and reference systems, this locality approximation leads to

$$\begin{aligned} U_p^0(r) &= U_p(r) - \hat{c}_p^+(0)\rho^+(r) - \hat{c}_p^-(0)\rho^-(r) \\ U_s^0(r) &= U_s(r) - \hat{c}_s^+(0)\rho^+(r) - \hat{c}_s^-(0)\rho^-(r) \end{aligned} \tag{2.8}$$

where we introduce the following variable definitions:

$$\hat{c}_p^+(0) = \left(\hat{c}_{pp}(0) + \hat{c}_{ps}(0)\right)/2\,;\ \hat{c}_s^+(0) = \left(\hat{c}_{ss}(0) + \hat{c}_{ps}(0)\right)/2\,;$$

$$\hat{c}_p^-(0) = \left(\hat{c}_{pp}(0) - \hat{c}_{ps}(0)\right)/2\,;\ \hat{c}_s^-(0) = \left(\hat{c}_{ps}(0) - \hat{c}_{ss}(0)\right)/2\,;\ \rho^+ = \rho_p + \rho_s;\ \rho^- = \rho_p - \rho_s.$$

The $\hat{c}(0)$ is conveniently viewed as the sum of a contribution due to the attractive site-site interactions, $\hat{c}^A(0) > 0$ and one due to the repulsive interactions, $\hat{c}^R(0) < 0$. Since it is usually the case that $\left|\hat{c}^R(0)\right| >> \left|\hat{c}^A(0)\right|$, the $\hat{c}^+(0)$ are dominated by the $\hat{c}^R(0)$'s. These terms serve as a restoring force such that for large (negative) $\hat{c}^+(0)$'s, one finds that $\rho^+(r)\sim 0$. Consequently, it is often expedient to include an undetermined multiplier term of the form $\int\lambda(r)\rho^+(r)dr$ in ΩW in equation (B.9) to constrain the system so that $\left(\rho_p + \rho_s\right)$ is a constant. When this constraint is enforced through $\delta W/\delta\rho^+ = \delta W/\delta\rho^- = \delta W/\delta U^0 = 0$, the expression for the fields becomes:

$$U_p^0(r) = U_p(r) - 2\hat{c}_p^{\xi}(0)\xi_p(r) + \eta(r)$$
$$U_s^0(r) = U_s(r) - 2\hat{c}_s^{\xi}(0)\xi_p(r) + \eta(r) \qquad (2.9)$$

where additional constant terms have been omitted. By splitting the $\hat{c}^{\xi}(0)$'s into repulsive and attractive contributions. The fields can now be written as:

$$U_p^0(r) = U_p(r) - \Xi_p\xi_p(r) - 2\Xi_p\eta(r) + \eta(r)$$
$$U_s^0(r) = U_s(r) + \Xi_s\xi_p(r) + 2\Xi_s\eta(r) + \eta(r) \qquad (2.10)$$

where

$$\Xi_p = \left(\hat{c}_{pp}^R(0) - \hat{c}_{ps}^R(0)\right); \Xi_s = \left(\hat{c}_{ss}^R(0) - \hat{c}_{ps}^R(0)\right);$$
$$\Xi_p = \frac{\Xi_{tot}}{2}(\hat{c}_{pp}^A - \hat{c}_{ps}^A); \Xi_s = \frac{\Xi_{tot}}{2}(\hat{c}_{ss}^A - \hat{c}_{ps}^A); \qquad (2.11)$$

$\eta(r)=\xi_p(r)/\Xi_{tot}$; and $\Xi_{tot}=\Xi_P+\Xi_S$. The Ξ's are related[22] to the Flory-Huggins χ-parameter through $\chi=\Xi_P+\Xi_S$. In addition, by making the symmetry assumptions that $\Xi_P=\Xi_S$, and that $\xi_p=\xi_s=0$ in the spirit of Flory-Huggins theory, we are led to the well known field commonly employed in standard SCF theory

$$U_p^0(r) = U_p(r) - \Xi\Xi\eta(r) + \eta(r)$$
$$U_s^0(r) = U_s(r) + \Xi\Xi\eta(r) + \eta(r). \qquad (2.12)$$

Of course, $\xi_p=\xi_s=0$ does not rigorously hold when there is asymmetry between monomeric and solvent structure. This effect is extreme for the case of athermal polymer brushes, where there is no solvent, or in a model where the solvent is treated as a continuum existing solely to make up the difference between Ξ_P and Ξ_{tot}. This is precisely the system studied in the MD simulations of Murat and Grest[15-18]. Since the solvent molecules are not explicitly considered, the direct correlation functions associated with

the solvent are zero resulting in $\xi_p = \hat{c}^R_{pp}(0;\langle\rho\rangle)$ and ξ_s=0. Thus, in our approach for the continuum solvent case, the fields become

$$\begin{aligned} U^0_p(r) &= U_p(r) - \hat{c}^R_{pp}(0;\langle\rho\rangle)\rho_P(r) - \omega(r) + \eta(r) \\ U^0_s(r) &= U_s(r) + \omega(r) + \eta(r) \end{aligned} \tag{2.13}$$

where the density of the reference system $\rho_{p,ref}= \langle\rho\rangle$ is explicitly denoted. In the SCMF theory, $\langle\rho\rangle$ would be 0 while, in the current study, $\langle\rho\rangle$ is determined through the average in equation (2.5). In the present investigation, we consider only the athermal solution where χ=0. We will study both the compressible, continuum solvent where η(r)=0, as well as, the incompressible limit where the Langrange multiplier η(r)≠0 enforces the incompressibility constraint of $\rho_{tot}\sigma^3$=1. Since we are dealing with tangent, hard-site chains, the $\hat{c}^R_{p,p}(0)$ can be found[21] from the equation of state for the bulk polymer of density $\langle\rho\rangle$. Finally, in order to model athermal, tethered chains in the presence of an explicit solvent, we take ξ_p=ξ_s=0 with incompressibility enforced.

3. Results and Discussion

To provide a basis of comparison with previous work we first treat our model with conventional SCF theory in the athermal limit for which the polymer and solvent fields in Eq. (2.12) reduce to

$$\begin{aligned} U^0_p(z) &= U_p(z) + \eta(z) \\ U^0_s(z) &= U_s(z) + \eta(z). \end{aligned} \tag{3.1}$$

It can be seen from this equation that the only molecular content left in these fields is the Lagrange multiplier η(z) that enforces the incompressibility constraint. These fields were used to solve for the density profiles of N=50 unit tethered chains with surface coverages

(chains/area), $\sigma_A a^2$, of 0.01, 0.03, 0.10 and 0.20, and of N=100 chains for $\sigma_A a^2$ of 0.03 and 0.07. As discussed earlier, our calculations were performed with a random-walk, ideal chain in the external field using the Fourier transform method discussed in Appendix A where 300 Fourier components were used for the N=50 chains and 600 components, for the N=100 chains. The results, which would be applicable to athermal, wet brushes are shown in Fig. 1. Although the chains become strongly stretched for the two largest σ_A's, it can be seen that the profiles are well described by parabolas. These are in good qualitative agreement with previous SCF results[9]; however, since most of the literature results are lattice calculations without finite extensibility, direct comparison is difficult.

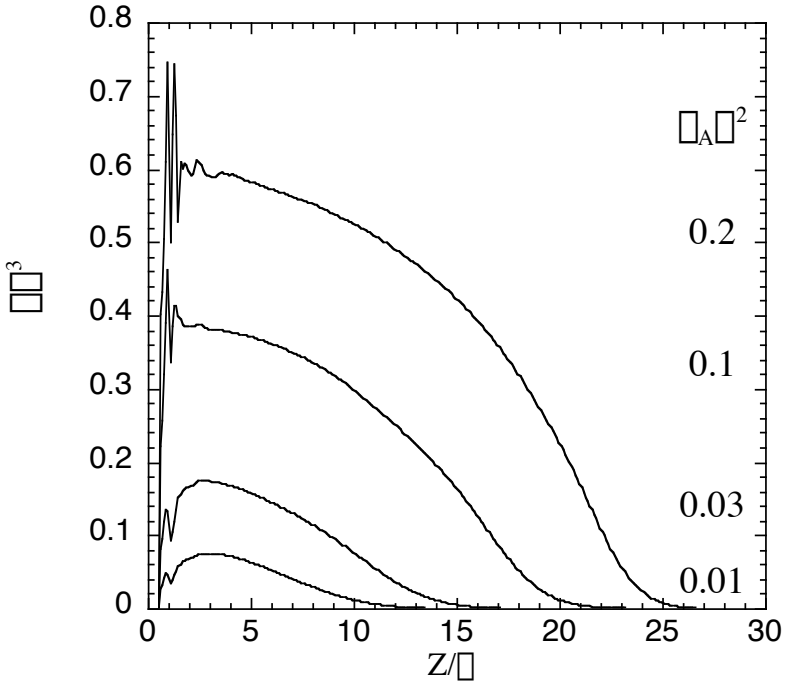

Figure 1: Conventional SCF (with finite extensibility) results for ideal chains for N=50. Surface coverages of $\sigma_A a^2$=0.01; 0.03; 0.1; 0.2.

In order to test the accuracy of our approach we will first make contact with the continuum solvent, MD simulations of Murat and Grest[14-18] who considered bead-spring model chains tethered to a hard wall for a range of surface coverages. No solvent molecules were explicitly treated in most of their simulations. Instead, solvent-induced, intramolecular attractions were introduced to mimic the effects of solvent quality. Here we will focus on the athermal simulations, corresponding to good solvent conditions. In our theory this implies that $\chi_p = \chi_s = 0$ in the equations developed in the previous section.

The appropriate fields to use in this case are depicted in Eq. (2.13) which, in the athermal limit, reduce to

$$\begin{aligned} U_p^0(r) &= U_p(r) - \hat{c}_{pp}^R(0;\langle\rho\rangle)\rho_P(r) + \xi(r) \\ U_s^0(r) &= U_s(r) + \xi(r) \end{aligned} \tag{3.2}$$

Note the presence of the extra term in the polymer field that arises when the direct correlation function, $\hat{c}_{ps}^R(0)$, vanishes as a result of the lack of solvent interactions in the system. We employed the polymer and solvent fields in Eq. (3.2) in two types of DFT calculations using the ideal and reference systems discussed earlier. In one case we envision the presence of ideal, gas-like solvent molecules whose only purpose is to ensure that $\rho_p(z) + \rho_s(z) = \text{constant}$. This incompressibility constraint is enforced through the Lagrange multiplier $\xi(z)$. The other case we consider more closely matches the simulation where no solvent molecules are present. This corresponds to putting ξ=0 in Eqs. (3.2) thereby allowing the system to be compressible.

In this investigation, we evaluated the polymer/polymer direct correlation function $\hat{c}_{pp}^{R}(0,\langle\rho\rangle)$ in Eq. (3.2) from the equation-of-state of a bead-spring polymer melt having a density of $\langle\rho\rangle$ corresponding to our reference state. The zero-wave-vector, direct-correlation function can be related to the isothermal compressibility $\kappa_T = \rho\left(\partial \ln V / \partial P\right)_T$ according to[21]

$$\langle\rho\rangle\hat{C}_{pp}\left(0,\langle\rho\rangle\right) = \frac{1}{N} - \frac{1}{\langle\rho\rangle k_B T \kappa_T} \tag{3.3}$$

The compressibility, and, hence, the direct correlation function, was obtained at each density from simulation data[28] for repulsive bead-spring chain melts and fit[21] to a Carnahan and Starling form

$$\frac{P}{\langle\rho\rangle k_B T} = \frac{1}{N} + \frac{K_1\eta + K_2\eta^2 + K_3\eta^3 + K_4\eta^4}{(1-\eta)^3} \tag{3.4}$$

where the packing fraction is $\eta = \pi\langle\rho\rangle/6$, and the coefficients, K_i, have a molecular weight dependence[21] given by

$$\begin{aligned} K_1 &= 4 - 2X - 1.248X^2 \\ K_2 &= -2 + 3.7028X + 3.976X^2 \\ K_3 &= -2.653X - 3.059X^2 \\ K_4 &= 0.64178X + 0.69164X^2 \end{aligned} \tag{3.5}$$

with the expansion variable $X = 1 - 1/N$.

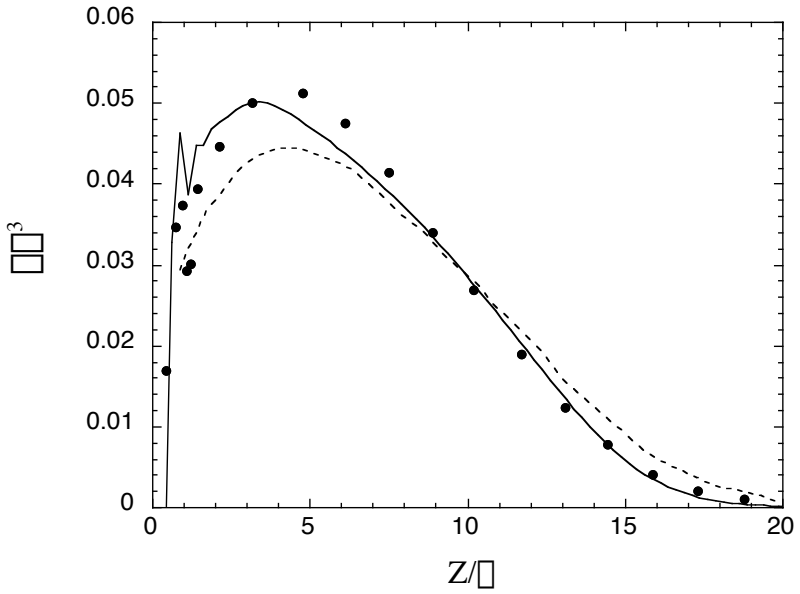

Figure 2: Athermal, excluded volume chains of 50 sites and surface coverage of $\theta_A\sigma^2$=0.01. DFT results of current study for $\Omega \neq 0$ (solid line) are compared to those of Murat and Grest[14-18] (circles) and to those of Carignano and Szleifer[10,11] (dashed line).

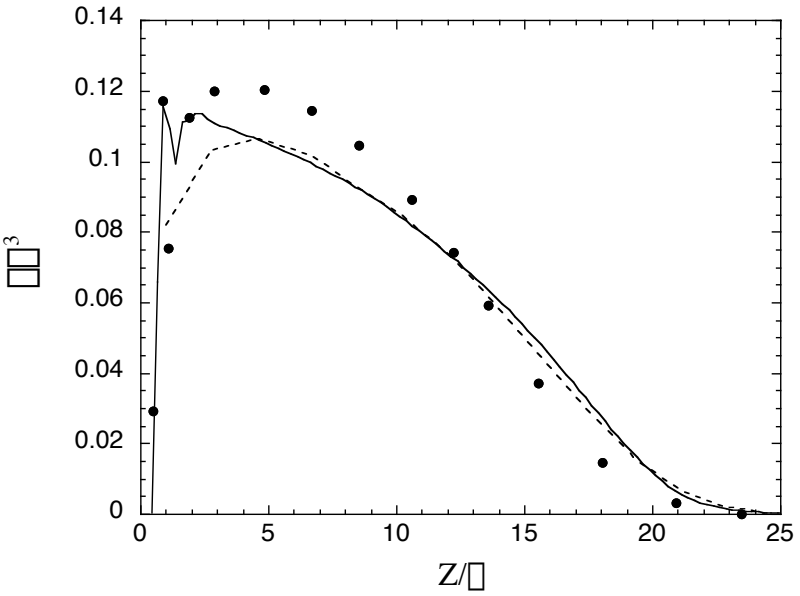

Figure 3: Athermal, excluded volume chains of 50 sites and surface coverage of $\theta_A\sigma^2$=0.03. Symbols as in Fig. 2.

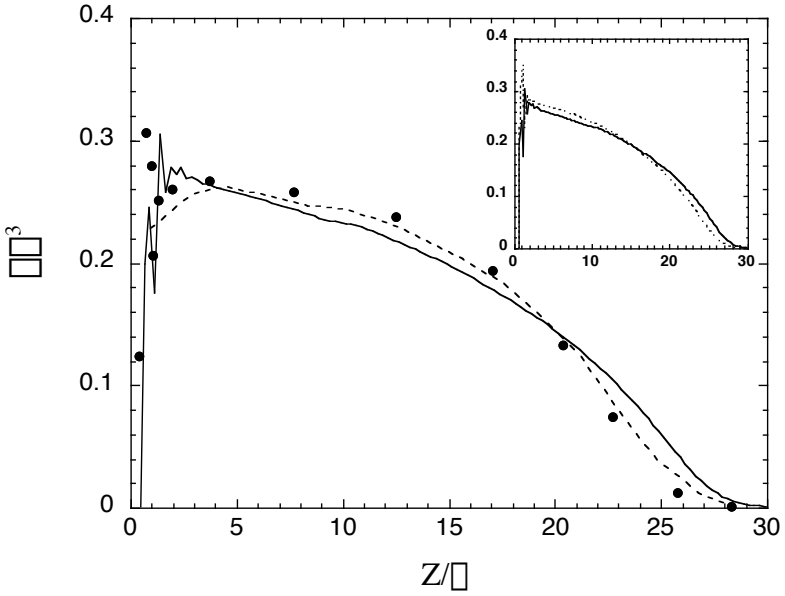

Figure 4: Athermal, excluded volume chains of 50 sites and surface coverage of $\square_A\square^2$=0.1. Symbols as in Fig. 2. The insert shows the effect of the incompressibility constraint. The solid line is the □≠0 result as in the main plot while the dashed line is the □=0 result.

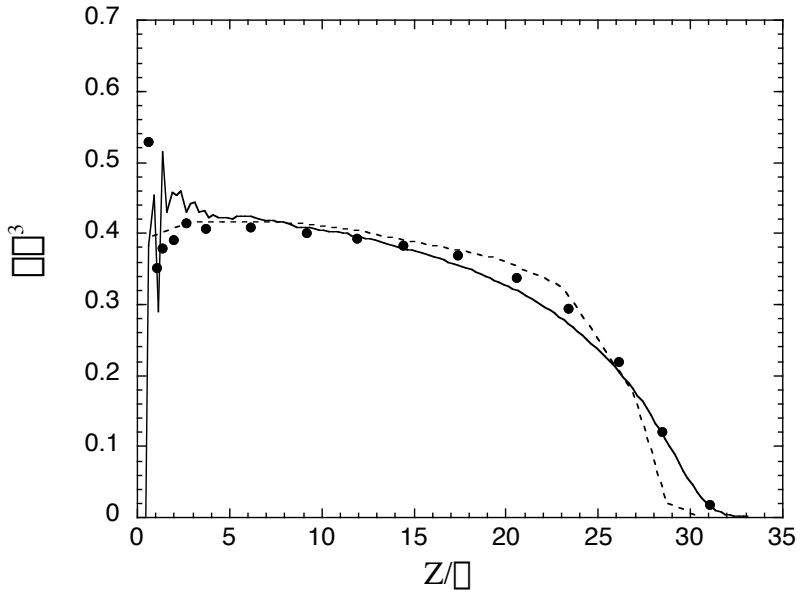

Figure 5: Athermal, excluded volume chains of 50 sites and surface coverage of $\square_A\square^2$=0.2. Symbols as in Fig. 2.

The results of our theory for continuum solvents of N=50 are shown in Figs. 2 through 5 along with the SCMF calculations performed earlier by Carignano and Szleifer[10]. In these figures it can be seen that the present DFT theory is in excellent agreement with the continuum solvent simulations of Murat and Grest. As the dimensionless surface coverage $\Sigma_A\sigma^2$ increases from 0.01 to 0.20, both the theoretical and MD profiles become more nonparabolic and extended. Furthermore, the results of the present DFT theory are very close to those of the SCMF calculations. This is significant since the SCMF calculations were based on a SAW ideal chain model whereas, in our approach, a theory based on a random-walk, ideal chain was developed. This is of practical importance since the demands of the numerical, random-walk calculation are relatively modest, each profile typically taking only a few minutes to generate on a typical workstation.

Interestingly, the enforcement of incompressibility in our theory has very little effect on the density profile as can be seen from the insert in Fig. 4. This is certainly not the case for conventional SCF theory where the density profiles are strongly compressed by the Π-field. Both the Π and the $\hat{c}^R(0)$ contributions to the field in our incompressible DFT calculations serve to flatten and extend the density profile. Apparently, in our compressible DFT calculations the $\hat{c}^R(0)$ contribution is much stronger than that of $\Pi(z)$ making the latter term irrelevant; however, in conventional SCF theory where $\hat{c}^R(0)$ is absent, as indicated in Eq. (3.1), the more modest chain perturbation due to $\Pi(z)$ is made apparent.

Examination of Figs. (4) and (5) reveals that at high surface coverages, the polymer profile tends toward a step function where the polymer density is constant within

the tethered layer and zero outside. Such a step profile was assumed in early scaling theories of polymer brushes[1,2]. From these scaling approaches it can be demonstrated that the layer thickness obeys the relation $\langle z \rangle \sim N\sigma_A^{1/3}$ with respect to the chain length and surface coverage. A check of this prediction with our theory, along with the MD and SCMF results, is depicted in Fig. (6). It can be observed from this figure that the curves from both our theory and the Murat and Grest MD simulations, approach $\langle z \rangle \mu\ N\sigma_A^{1/3}$ for large surface coverages and chain lengths in accordance with scaling predictions. Over this same range it appears that the SCMF results have still not reached the brush-like scaling regime[11].

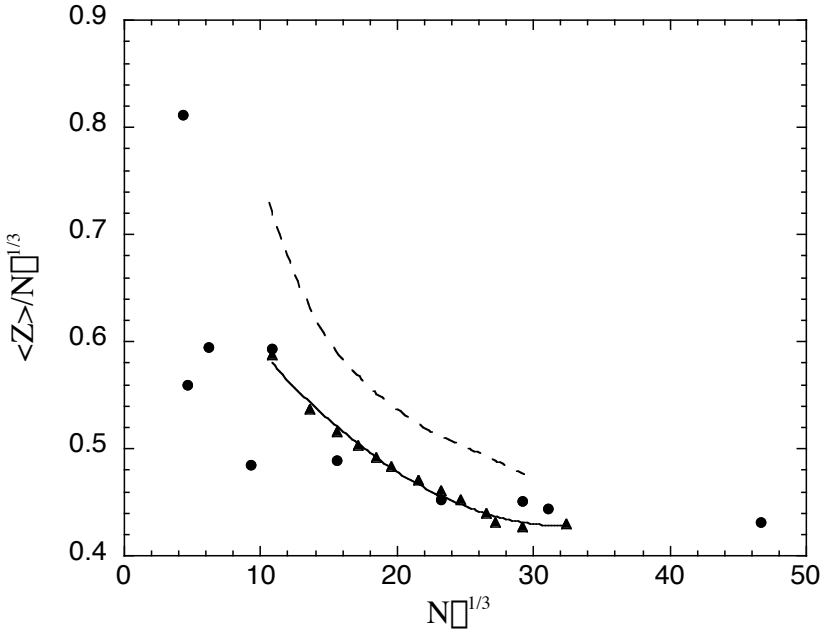

Figure 6: Scaling of average site distance from wall for athermal, excluded volume chains. The solid line is the result of $\sigma \neq 0$, DFT for the cases of N=50, $\sigma_A\sigma^2$=0.01 to 0.2 (11 points); N=100, $\sigma_A\sigma^2$=0.02; N=150, $\sigma_A\sigma^2$=0.01. The dashed line represents the results of Carignano and Szleifer[10,11]. The circles are the results of Murat and Grest[14-18].

Thus far we have only considered tethered chains in a continuum solvent. We know from MD simulations[26] and PRISM theory[27] that in bulk polymer solutions, the presence of explicit solvent molecules significantly reduces the radius of gyration of the polymer compared to the continuum solvent. Thus an explicit athermal solvent is still a good solvent for the polymer, but not as good as a continuum solvent. One might expect a similar effect of explicit solvent molecules in a tethered chain system. This is indeed what was observed in the MD simulations of Grest[17] who studied tethered polymers in chain solvents of various lengths. Let us consider how the fields in Eq. (2.10) are modified due to the presence of explicit solvent molecules. Now the direct correlation functions associated with the solvent are no longer zero, and, as a result, the term ξ_p no longer reduces to $\hat{c}^R_{pp}(0)$ as in Eq. (2.13) but is a balance between polymer/polymer and polymer/solvent direct correlation functions. A similar argument applies for the ξ_s term. As discussed earlier, one can argue that the various direct correlation functions balance each other so that, to first approximation, $\xi_p \approx \xi_s \approx 0$. This leads to the fields in Eqs. (2.12) or (3.1) that are commonly employed in SCF calculations, and also used in the present investigation in Fig. (1) for N=50.

In order to compare with the athermal MD simulations of Grest[17] we performed (finite extensibility) SCF calculations on tethered chains of N=100 for an explicit monomeric (N=1) solvent using the fields in Eq. (3.1). In Figs. (7) and (8) these results are compared at two surface coverages with the corresponding tethered chains in a continuum solvent, using the fields in Eq. (3.2), along with the relevant MD simulations. Not surprisingly, the agreement between our DFT theory and simulation for the N=100 tethered chains in continuum solvent is excellent – just as it was for N=50 chains. What is

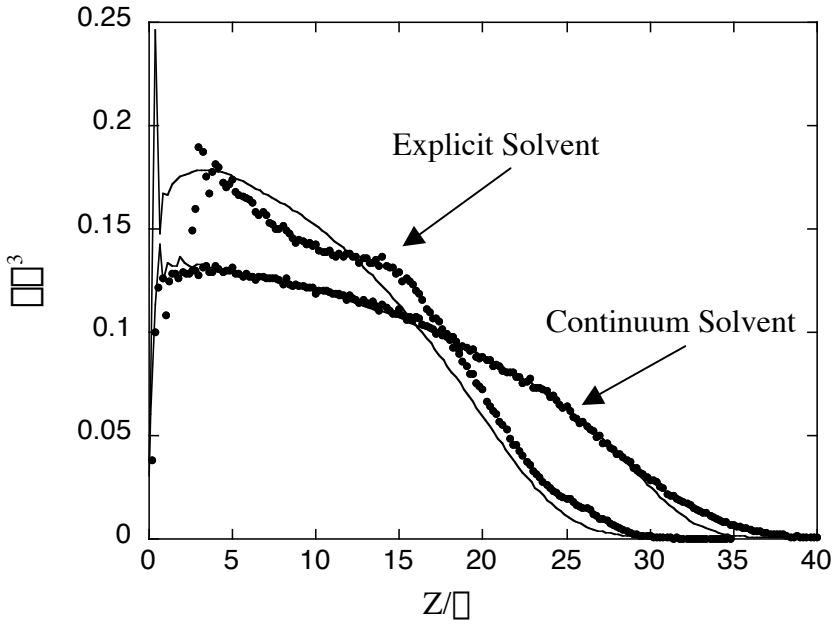

Figure 7: Comparison of explicit and continuum solvents. The symbols are the results of computer simulation and the curves are those of DFT. The tethered chains are of length 100 and the explicit solvent is monatomic. The surface coverage is $\rho_A\sigma^2$=0.03. Near-wall simulation details are not shown.

remarkable, however, is that the simple SCF theory does a very good job of describing the density profiles for the tethered chains with explicit solvent molecules present. The effect of local packing can be seen in the inset. Within 6□ of the wall, the "solvation-shell" structure seen in high density liquids is manifest. In reality, the total density is not a constant with respect to distance from the wall, and, since the diameters of the solvent and monomer are equal in the explicit solvent simulations of Ref 17, the layering of the total density is pronounced. Consequently, the structure seen in the polymer density in the six-sigma region is strongly influenced by the structure of the total density.

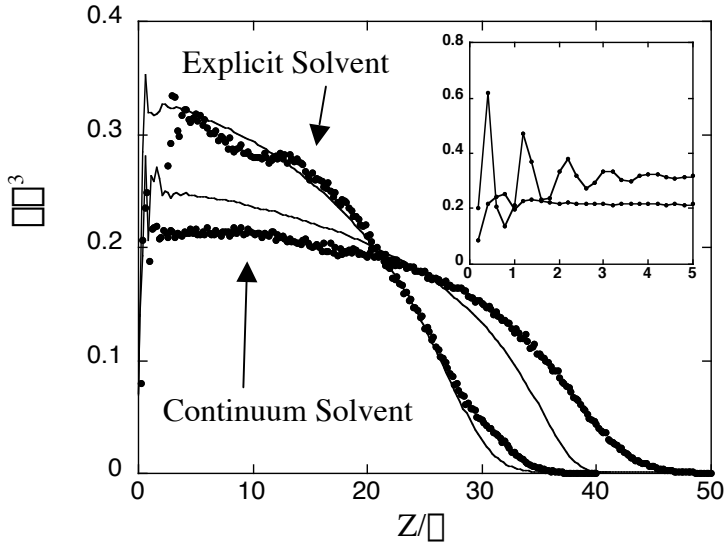

Figure 8: Comparison of explicit and continuum solvents. Symbols as in Fig. 7 except $\rho_A\sigma^2$=0.1. Near-wall simulation details are shown in the insert, but not in the main figure.

For walls of sufficiently small separations, the density profiles of the tethered chains on the two walls overlap. This is seen in Fig. (9) where the MD simulations of Murat and Grest[18] are well described by the DFT results. Of course, solvent effects would strongly affect the wall-wall interactions. In particular, the presence of explicit solvent would delay the overlap of the profiles until smaller wall separations. This is seen in the predictions of DFT for explicit solvents shown in Fig. (10).

4. Conclusions

The primary intent of the current study is to formulate a general theory for tethered polymer chains based on atomic level interactions that is capable of describing both long and short range structure. We find if we sacrifice information regarding the short-range packing, then our general DFT formalism reduces to SCMF theory in the case of continuum-solvent brushes, and to SCF theory when the solvent molecule is treated explicitly. The assumptions necessary for this simplification include: locality of the

fields, symmetry in the repulsive direct correlation functions, and incompressibility. By going through the DFT route, it becomes apparent that the theory can be implemented numerically through a random walk, ideal-chain model provided that the reference state is chosen appropriately. When applied to the continuum solvent problem, this approach gave results in agreement with SCMF theory and MD simulation. It should be emphasized, however, that in our formulation this agreement was achieved without resorting to a single chain Monte Carlo simulation as is required in SCMF theory.

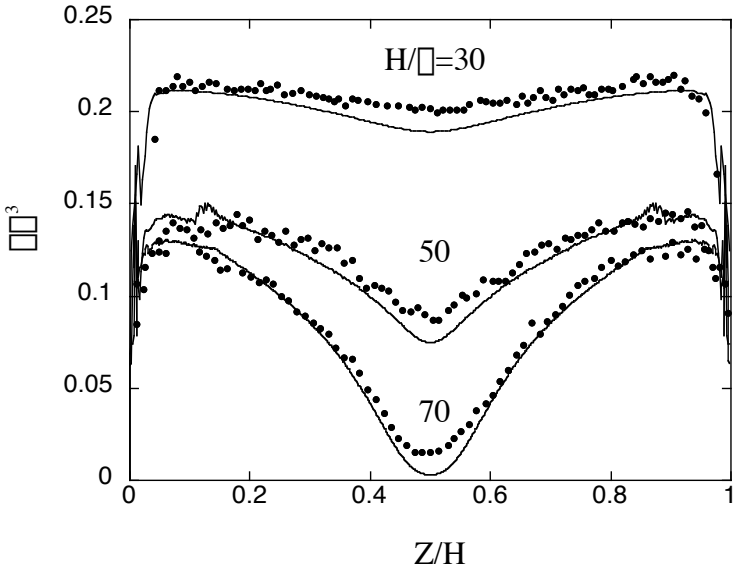

Figure 9: Athermal (continuum-solvent) excluded volume chains of 100 sites with σ_A^2=0.03 and finite wall separations, H/σ = 30, 50, and 70 as indicated. The lines are the results of the DFT with $\xi \neq 0$ and the circles are the MD results of Grest.

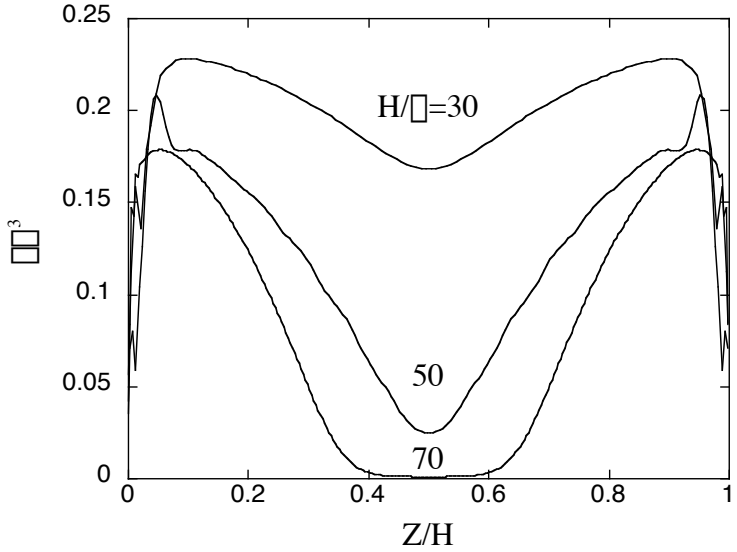

Figure 10: Athermal, explicit-solvent, excluded-volume chains of 100 sites with $\rho_A\sigma^2$=0.03 and finite wall separations, H/σ = 30, 50, and 70 as indicated. The lines are the results of the DFT with ξ≠0.

In general, the repulsive, direct-correlation functions of polymer and solvent enter DFT theory through the fields in Eq. (2.10). However, in the case of tethered, bead-spring polymers in an athermal, monatomic solvent, we found that the symmetry between the monomer and solvent structure causes the repulsive, direct-correlation functions to drop out of the problem. Beyond a distance of about six monomer diameters from the wall, the SCF-limit of the DFT theory (which includes finite extensibility) gives an accurate description of the simulations of Grest in the presence of explicit solvent molecules. In the case of more complex polymer and solvent models the specific direct correlation functions would need to be included in the calculation.

Our DFT theory, as formulated in the Appendices, is developed for a polymer model where each monomer and each solvent molecule consists of a single site. Provided

there is no long range intramolecular excluded volume, the ideal polymer chain is Markovian. This permits the density profile to be calculated numerically as outlined in Appendix A. More realistic models, that faithfully reproduce monomeric and solvent architecture with multiple sites, would give a more accurate representation of the local structure. Such a model can be treated with DFT methods, however, even when the excluded volume is screened, the ideal chain is no longer Markovian. In other words, the position of the nth site on a chain will depend not just on the (n-1)st site, but may also on the (n-2) and (n-3)st sites as well. It seems likely that a model, such as the "rotational isomeric state" model containing local architectural details, would be amenable to numerical solution if long range excluded volume effects are absent.

Throughout this work we have assumed that the various direct correlation functions are of zero range and, consequently, are proportional to delta functions. This assumption, when inserted into Eq. (2.2), leads to solvent and polymer fields that are local in the sense that the field at location z depends only on the density profile at this same location z, and not on the density at nearby locations. We expect that this locality approximation would lead to accurate predictions on long length scales, but would fail to accurately capture local packing effects near the wall. In the MD simulations of Murat and Grest, both with and without explicit solvent molecules, we see that the tethered chains do show significant local packing effects in the region within six monomer diameters of the wall. Thus the simple SCF and SCMF theories give remarkably good descriptions of tethered chains on long length scales. For many applications the near surface structure is important. For instance, the degree of solvent penetration to the wall or the pressure of a tethered chain on an opposing, bare wall would both be sensitive to the details of local

packing. This is similar to the case of untethered, free polymer chains near surfaces[21-23] where the calculation of, for example, surface tension is sensitive to details of the six-sigma wall region. In order to accurately probe this wall region, DFT theory needs to be implemented with nonlocal fields incorporating the finite range of the direct correlation functions.

Appendix A: Evaluation of the density profile from the ideal external field:

$$\rho(z)=F[U^0(z)]$$

The density profile, $\rho(z)$, of even a simple, ideal chain cannot be solved in closed form when the chain is interacting with an arbitrary external field, $U^0(z)$; however, the judicious use of Fourier transforms permits a convenient numerical solution. This approach is discussed in some generality in reference 21, and, in this appendix, the specific application to tethered chains is addressed.

Of particular importance for tethered chains is the maintenance of finite extensibility. One of the primary reasons that the lattice based treatment of self-avoiding chains fails to quantitatively agree with off-lattice simulations is that the lattice chains do not rigidly enforce finite extensibility. One may also speculate that the lack of finite extensibility in the Gaussian chains used in SCF theories of tethered chains would be as large a source of error as the neglect of some of the excluded volume contributions. The approach of the current work does enforce this constraint, and, as a consequence, our results are most easily compared to those of other off-lattice studies of chains of fixed bond length.

The density distribution of a given site on an un-tethered chain (for instance, the 4th site of a 6 site chain) can be decomposed into the product of two integrals

$$\rho_4(z_4) \propto I_{left}(z_4)\exp\left(-U^0(z_4)\right)I_{right}(z_4) \qquad (A.1)$$

where

$$I_{left}(z_4) = \int\int\exp\left[-U^0(z_1)\right]\delta\left(|\underline{r}_2-\underline{r}_1|-b\right)\exp\left[-U^0(z_2)\right] \times \delta\left(|\underline{r}_3-\underline{r}_2|-b\right)\exp\left[-U^0(z_3)\right]\delta\left(|\underline{r}_4-\underline{r}_3|-b\right)d\underline{r}_1 d\underline{r}_2 d\underline{r}_3 \qquad (A.2)$$

and

$$I_{right}(z_4) = \int\int \delta(|\underline{r}_5 - \underline{r}_4| - \sigma)\exp\left[-U^0(z_5)\right]\delta(|\underline{r}_6 - \underline{r}_5| - \sigma)\exp\left[-U^0(z_6)\right]d\underline{r}_5 d\underline{r}_6 ; \quad (A.3)$$

the fields are expressed in units of k_BT; k_B is the Boltzmann constant; and T is the temperature.

Such integrals can be evaluated with Fourier transforms. Consider I_{right} as an example. Working from right to left:

$$\exp\left[-U^0(z_6)\right] = \frac{a_0}{2} + \sum_{n=1}^{\infty} a_n \cos\left(\frac{n\pi z_6}{L}\right) \quad (A.4)$$

where 2L is the distance between the two walls of the pore; the origin of z_6 has been shifted so the function is even; and

$$a_n = \frac{1}{L}\int_{-L}^{L}\exp\left[-U^0(z)\right]\cos\left(\frac{n\pi z}{L}\right)dz \ . \quad (A.5)$$

The right most delta function can be expressed as

$$\delta(|\underline{r}_6 - \underline{r}_5| - \sigma) = \frac{1}{8\pi^3}\int_{-\infty}^{\infty}\exp\left[i\underline{k}\bullet(\underline{r}_6 - \underline{r}_5)\right]\frac{\sin(k\sigma)}{k\sigma}\,d\underline{k} \quad (A.6)$$

where $i = \sqrt{-1}$. The integral over $\underline{r}_6$ is then

$$\begin{aligned}
\int\delta(|\underline{r}_6 - \underline{r}_5| - \sigma)\exp\left[-U^0(z_6)\right]d\underline{r}_6 &= \int_{-L}^{L}\left[\frac{1}{8\pi^3}\int_{-\infty}^{\infty}\exp\left[i\underline{k}\bullet(\underline{r}_6 - \underline{r}_5)\right]\frac{\sin(k\sigma)}{k\sigma}\,d\underline{k}\right]\exp\left[-U^0(z_6)\right]d\underline{r}_6 \\
&= \frac{1}{2\pi}\int_{-\infty}^{\infty}\exp\left[-ik_z z_5\right]\frac{\sin(k_z\sigma)}{k_z\sigma}\left[\int_{-L}^{L}\exp\left[ik_z z_6\right]\exp\left[-U^0(z_6)\right]dz_6\right]dk_z \\
&= \frac{1}{2\pi}\int_{-\infty}^{\infty}\exp\left[-ik_z z_5\right]\frac{\sin(k_z\sigma)}{k_z\sigma}\left[\sum_{n=-\infty}^{\infty} a_n\delta(|k_z| - \frac{n\pi}{L})\right]dk_z \\
&= \frac{a_0}{2} + \sum_{n=1}^{\infty} a_n \frac{\sin(n\pi\sigma/L)}{n\pi\sigma/L}\cos\left(\frac{n\pi z_5}{L}\right) \quad (A.7)
\end{aligned}$$

The delta function $\delta(|k_z|-n\pi/L)$ arises from treating $\exp(-U^0(z))$ as an even, periodic function from $z= -\infty$ to ∞. Only wavelengths commensurate with the function's period (2L) contribute to the integral, which generates the finite Fourier transform.

The result of equation (A.7) is a function of z_5 which is then multiplied by $\exp(-U^0(z_5))$, taken back into Fourier space to be multiplied by the next delta function, and so on until the integral is evaluated.

When starting from the tethered end, an extra site is added to equation (A.2) and fixed to the wall with a delta function:

$$\begin{aligned}
\int I(z_0)\,\delta\left(|\underline{r}_1-\underline{r}_0|-\right)d\underline{r}_0 &= \int_{-L}^{L}\delta(x_0)\,\delta(y_0)\,\delta(z_0-L)\left[\frac{1}{8\pi^3}\int_{-\infty}^{\infty}\exp\left[i\underline{k}\bullet\left(\underline{r}_1-\underline{r}_0\right)\right]\frac{\sin(k\pi)}{k\pi}d\underline{k}\right]d\underline{r}_0 \\
&= \frac{1}{2\pi}\int_{-\infty}^{\infty}\exp\left[ik_z r_1\right]\frac{\sin\left(k_z\pi\right)}{k_z\pi}\left[\int_{-L}^{L}\exp\left[-ik_z z_0\right]\delta(z_0-L)dz_0\right]dk_z \\
&= \frac{1}{2\pi}\int_{-\infty}^{\infty}\exp\left[-ik_z z_1\right]\frac{\sin\left(k_z\pi\right)}{k_z\pi}\left[2\pi\sum_{n=-\infty}^{\infty}\cos\left(k_z L\right)\delta\left(|k_z|-\frac{n\pi}{L}\right)\right]dk_z \\
&= 1+\sum_{n=1}^{\infty}\frac{\sin(n\pi/L)}{n\pi/L}2\cos(n\pi)\cos\left(\frac{n\pi z_1}{L}\right) \qquad \text{(A.8)}
\end{aligned}$$

Equation (A.8) is a real space function which is then multiplied by $\exp(-U^0(z))$; taken into Fourier space; multiplied by $\sin(n\pi/L)/(n\pi/L)$; etc., just as for I_{right}. The product of the two integrals, I_{right} and I_{left} is multiplied by $\exp(-U^0(z))$ and normalized. For computational convenience, the trigonometric functions needed in the Fourier transforms are calculated at each k and at each real-space grid-point near the beginning of the program and stored in memory to be used during the iteration process.

Although a straightforward enough algorithm, the above is rather notationally cumbersome. As is often the case, denoting the integrals as graphs clarifies the mathematical derivations. In particular, equation (A.1) can be rewritten as

$\rho_4(z)\mu$ 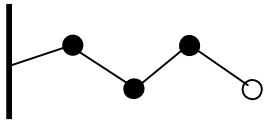 $\exp(-U^O(z))$ 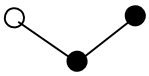 (A.9)

where the black circles are $\exp(-U^O(z))$ circles which have been integrated over; the white circles are 1-circles which have not been integrated over; the thin lines are displaced delta functions, $\delta(|\underline{r}_1-\underline{r}_2|-\sigma)$; σ is the bond length; the heavy vertical line is the hard wall; and density profile of this site, $\rho_4(z)$, is normalized so that the surface coverage, θ_A, is $\int\rho_4(z)\,dz$. The total density profile (i.e., the functional $F[U^0(z)]$) is then the sum over the density profiles for each site along the chain. All of the calculations reported here were performed in slit pores of large width with identical polymer coatings on each wall.

By switching back and forth between real and Fourier space, each of the two graphs in equation (A.9) can be found as a function of z. One of the resulting distributions will peak near the wall and have a tail extending, in this case, to a distance of 4σ. The other will peak away from the wall and have a tail towards the wall. For the case illustrated above this would not be problematic: the product of the two distributions would have a significant overlap region and, when properly normalized, $\rho_4(z)$ would result. However, if the right-most graph in Fig. (A.9) was, say, 100 sites long instead of 2, numerical problems would ensue. The right-hand distribution resulting from the procedure described above would be essentially zero over the range where the left-most

distribution is non-zero. Since the integrated value of $\rho_4(z)$ must be non-zero, the overlap of these numerically small tails must be included in the calculation.

The calculations are performed starting from the density profile of the free end, $\rho_{End}(z)$, and working in towards the sites near the tethering point. The area of each overlap region is calculated (before normalization to ρ_A). When this area drops to less than 10^{-8}, say for site i, then the density profile for site i+1 is used to approximate the density both for site i and for all subsequent sites. In particular, if the peak in $\rho_{i+1}(z)$ occurs at z_{i+1} and the peak in $\rho_1(z)$ is approximated as occurring at 0.25, then the peak in $\rho_j(z)$ would occur at $z_j = 0.25+(z_{i+1}-0.25)(j-1)/i$. Consequently, $\rho_j(z)$ was approximated as $\rho_{i+1}(0.25+(z-0.25)i/(j-1))$ for those sites in the low overlap area (except for $\rho_1(z)$ which was taken to be a constant between the wall and its maximum extension of 0.5σ). The grid spacing in the z-direction was 0.25σ.

Such, then, is the method we used to calculate the density profile of the polymer from the external field, and the density profile of the solvent, $\rho_s(z)$, is the comparatively trivial

$$\rho_s(z) = \rho_{s,bulk} \exp\left[-U_s^0(z)\right] \qquad (A.10)$$

where $\rho_{s,bulk}$ is the density of the solvent in the bulk which is in equilibrium with the inhomogeneous solvent; and $U_s^0(z)$ is the ideal external field of the solvent (in units of k_BT).

Appendix B: Evaluation of the ideal external field from the density profile: $U^0(z)=G[\rho(z)]$.

Consider the energy, E, of a polymer/solvent system in the presence of external fields:

$$dE = TdS - PdV + \mu_p dn_p + \mu_s dn_s + \int_V \rho_p(r) U_p(r) d\underline{r} + \int_V \rho_s(r) U_s(r) d\underline{r} \qquad (B.1)$$

where T is the temperature; S, the entropy; P, the pressure; V, the volume; μ, the chemical potential; n, the number of sites; $\rho(r)$, the site density; and U(r), the external field. The integrals are over the system volume; "p" denotes "polymer"; and "s" denotes solvent. The $\rho(r)$'s are constrained so that $n = \int_V \rho(r) d\underline{r}$.

From the definition $E^* = E - \int_V \rho_p(r) U_p(r) d\underline{r} - \int_V \rho_s(r) U_s(r) d\underline{r}$, one has

$$dE^* = TdS - PdV + \int_V \rho_p(r) \Delta\mu_p(r) d\underline{r} + \int_V \rho_s(r) \Delta\mu_s(r) d\underline{r} \qquad (B.2)$$

where $\Delta\mu(r)=\mu-U(r)$. The Helmholtz free energy, A, is then A=E*-TS, or

$$dA = -SdT - PdV + \int_V \rho_p(r) \Delta\mu_p(r) d\underline{r} + \int_V \rho_s(r) \Delta\mu_s(r) d\underline{r} \qquad (B.3)$$

Finally, the Grand Potential Free Energy is $\Omega = A - \int_V \rho_p(r) \Delta\mu_p(r) d\underline{r} - \int_V \rho_s(r) \Delta\mu_s(r) d\underline{r}$, or,

$$d\Omega = -SdT - PdV - \int_V \rho_p(r) \Delta\mu_p(r) d\underline{r} - \int_V \rho_s(r) \Delta\mu_s(r) d\underline{r} \qquad (B.4)$$

At fixed T,V, and μ(r)'s, Ω will be minimized. If constraints are added to the system to force the densities away from equilibrium, the resulting Grand Potential Free Energy, denoted $W[\rho_p(r),\rho_s(r)]$, will be greater that Ω, and

$$\Omega = \underset{\rho_p(r),\rho_s(r)}{\text{Min}} W\left[\rho_p(r),\rho_s(r)\right]. \qquad \text{(B.5)}$$

The heart of DFT theory (and, by extension, SCF theory) is the development of an expression for the functional $W[\rho_P(r),\rho_S(r)]$ which is then minimized with respect to $\rho_P(r)$ and $\rho_S(r)$. These density profiles which minimize the free energy functional are the equilibrium densities and the value of W[…] at the minimum is Ω. The only approximations in such an approach are those associated with the form of W[…].

A straightforward approach to developing an approximation for W[…] employs a functional Taylor series of the Helmholtz Free Energy in terms of the densities and at constant volume and temperature:

$$A = A_{ref} + \int_V \Delta\mu_{s,ref}\,\Delta\rho_s(r)\,d\underline{r} + \int_V \Delta\mu_{p,ref}\,\Delta\rho_p(r)\,d\underline{r} \qquad \text{(B.6)}$$

$$+ \frac{1}{2}\iint_V \left(A''_{pp}(r-r')\,\Delta\rho_p(r)\,\Delta\rho_p(r') + 2A''_{ps}(r-r')\,\Delta\rho_p(r)\,\Delta\rho_s(r') + A''_{ss}(r-r')\,\Delta\rho_s(r)\,\Delta\rho_s(r') \right) d\underline{r}\,d\underline{r}'$$

where "ref" denotes the homogeneous, reference liquid about which the expansion is performed; $\Delta\rho(r) = \rho(r)-\rho_{ref}$; and A'' is the second functional derivative of A with respect the indicated $\rho(r)$'s. Since $A'=\mu$, then $A''=\Delta\mu/\Delta\rho$ and since $\Delta\mu/\Delta\rho = \Delta\mu(r-r')+\Delta\rho h(r-r')$, a definition of the direct correlation function, c(r), as $\Delta\mu/\Delta\rho=\rho^{-1}(r-r')/\rho - c(r-r')$ is consistent with liquid state theory. Here ρ^{-1} is the functional inverse of the single chain correlation function for the PP case, is 0 for the PS case, and is $\delta(r-r')$ for the SS case. The pair correlation function, g(r), is h(r)+1. In particular,

$$A''_{pp}(r,r') = \frac{\delta^{-1}(r-r')}{\rho_p} - c_{pp}(r,r')$$
$$A''_{ps}(r,r') = -c_{ps}(r,r') \qquad \text{(B.7)}$$
$$A''_{ss}(r,r') = \frac{\delta(r-r')}{\rho_s} - c_{ss}(r,r').$$

Higher order terms in equation (B.6) are important, and, in order to correct for these terms, the Free Energy of an "ideal" system, denoted by "0", is also expanded and the difference taken with equation (B.6). This yields

$$\left(A - A^0\right) = \left(A_{ref} - A^0_{ref}\right) + \sum_{i=s,p}\int_V \left(\rho_{i,ref} - \rho^0_{i,ref}\right)\omega_i(r)\,d\underline{r} \qquad \text{(B.8)}$$
$$-\frac{1}{2}\sum_{i,j=s,p}\iint_V c_{i,j}(r,r')\omega_i(r)\omega_j(r')\,d\underline{r}\,d\underline{r}' + \frac{1}{2}\iint_V \frac{\left(\delta^{-1}(r,r') - \delta_0^{-1}(r,r')\right)}{\rho_{p,ref}}\omega_p(r)\omega_p(r')\,d\underline{r}\,d\underline{r}'$$

and the fundamental approximation in DFT theory is that the higher order terms have been negated by taking this difference. Of course, since the ideal and reference systems have been loosely defined at this point, it is difficult to evaluate the accuracy of this approximation; in particular, the "closer" the ideal system is to the fully interacting system, the better the approximation. We have allowed for a difference in δ^{-1} for the real and ideal systems; however, as long as the real and ideal chains are of equal length, the integrated values of the two δ^{-1} will be equal to 1/(chain length).

The Helmholtz Free Energies in (B.8) can now be changed to W[…]'s:

$$\Delta W = \Delta W^0 - \sum_{i=s,p}\int_V \left(\rho_i(r) - \rho_{i,ref}\right)\omega_i(r)\,d\underline{r} + \sum_{i=s,p}\int_V \left(\rho^0_i(r) - \rho^0_{i,ref}\right)\omega_i(r)\,d\underline{r} \qquad \text{(B.9)}$$
$$-\frac{1}{2}\sum_{i,j=s,p}\iint_V c_{i,j}(r,r')\omega_i(r)\omega_j(r')\,d\underline{r}\,d\underline{r}' + \frac{1}{2}\iint_V \frac{\left(\delta^{-1}(r,r') - \delta_0^{-1}(r,r')\right)}{\rho_{p,ref}}\omega_p(r)\omega_p(r')\,d\underline{r}\,d\underline{r}'$$

where $\Delta W = W - W_{ref}$. In order to minimize W (or, equivalently, ΔW) with respect to $\omega(r)$, the ideal system must be evaluated.

The ideal system we consider here is that of freely jointed chains and a point particle solvent. The density profiles can be related to W^0 through (B.4) where it is indicated that $\delta W/\delta\rho = \xi$. From the generalization of equation (A.1), it can be shown that

$$W^0 = \int\cdots\int \exp\left[\sum_{i=1}^{N} \xi_p^0(r_i)\right] S(\underline{r}_1 \cdots \underline{r}_N)\, d\underline{r}_1 \cdots d\underline{r}_N + \int \exp\left(\xi_s^0(r)\right) d\underline{r} \qquad \text{(B.10)}$$

where N is the number of sites on a chain and S(…) is the product of delta functions which enforces the bonding constraints. The ideal chemical potentials, ξ^0, are defined so that $N\xi_p^0 = \ln(\rho_p)$ and $\xi_s^0 = \ln(\rho_s)$.

In general, the $\xi^0(r)$'s cannot be expressed as a functional of the $\rho(r)$'s, and, as a result, the minimization of βW must be performed as a constrained minimization. This is done through the equations $\delta W/\delta\xi^0=0$ and $\delta W/\delta\rho=0$ where the expression (B.10) is used for W^0. The former of these yields $\rho(r)=F[U^0(r)]$ which was the subject of appendix A, and the latter yields

$$\begin{aligned} U_p^0(r) &= U_p(r) - \sum_{i=s,p} \int c_{p,j}(r - r')\,\Delta\rho_i(r')\, d\underline{r}' + \int \frac{\left(\xi^{-1}(r - r') - \xi_0^{-1}(r - r')\right)}{\rho_{p,ref}}\,\Delta\rho_p(r')\, d\underline{r}' \\ U_s^0(r) &= U_s(r) - \sum_{i=s,p} \int c_{s,j}(r - r')\,\Delta\rho_i(r')\, d\underline{r}' \end{aligned} \qquad \text{(B.11)}$$

where constant terms have been dropped. This equation is reasonably general; neither the ideal nor the reference system is specified. In the body of the paper it is used as a starting point for the analysis of tethered chains.

References

1. S. Alexander, J. Phys. (Paris) **38**, 983 (1977).
2. P. G. de Gennes, Macromolecules **13**, 1069 (1980).
3. J. M. H. M. Scheutjens and G. J. Fleer, J. Phys. Chem. **83**, 1619 (1979).
4. T. Cosgrove, T. Heath, B. van Lent; and J. M. H. M. Scheutjens, Macromolecules **20**, 1692 (1987);
5. K.R. Shull, J. Chem. Phys. **94**, 5723 (1991).
6. R. Baranowski and M. D. Whitmore, J. Chem. Phys. **108**, 9885 (1998).
7. M. Laradji, H. Guo, and M. J. Zuckermann, Phys. Rev. E **49**, 3199 (1994).
8. J.I. Martin and Z.G. Wang, J. Phys. Chem. **99**, 2833 (1995).
9. S.T. Milner, J. Chem. Soc. Faraday Trans. **86** 1349 (1990); S. T. Miller, T. A. Witten, and M. E. Cates, **21**, 2610 (1988).
10. M. A. Carignano and I. Szleifer, J. Chem. Phys. **98**, 5006 (1993);
11. I. Szleifer and M. A. Carignano, Adv. Chem. Phys. **94**, 165 (1995); I. Szleifer and M. A. Carignano, Macromol. Rapid Commun. **21**, 423 (2000).
12. S. T. Milner, Science **251**, 905 (1991).
13. A. Halperin, M. Tirrell, and T.P. Lodge, Adv. Polym Sci. **100**, 31, (1991).
14. G. S. Grest and M. Murat, in *Monte Carlo and Molecular Dynamics Simulations in Polymer Science*, ed. K. Binder (Oxford Univ. Press, NY, 1995), p 476.
15. M. Murat and G. S. Grest, Macromolecules **22**, 4054 (1989).
16. G. S. Grest and M. Murat, Macromolecules **26**, 3108 (1993).
17. G. S. Grest, J. Chem. Phys. **105**, 5532 (1996).

18 M. Murat and G. S. Grest, Phys. Rev. Lett. **63**, 1074 (1989); G.S. Grest, Private Communication.

19. P.Y. Lai and K. Binder, Makromol. Chem. Macromol. Symp. **65**, 189 (1993) and references there in.

20. D. Chandler, J. D. McCoy, and S. J. Singer, J. Chem. Phys. **85**, 5971 (1986).

21. J.D. McCoy, M.A. Teixeira, and J.D. Curro, J. Chem, Phys. **114**, 4289 (2001).

22. S.K. Nath, J.D. McCoy, J.G. Curro, and R.S. Saunders, J. Poly. Sci. B: Poly. Phys., **33**, 2307 (1995); S.K. Nath, J.D. McCoy, J.G. Curro, and R.S. Saunders, J. Chem. Phys. **106**, 1950 (1997); S.K. Nath, J.D. McCoy, J.G. Curro, and R.S. Saunders, J. Chem. Phys. **108**, 3023 (1998).

23. J.B. Hooper, J.D. McCoy, and J.G. Curro, J. Chem. Phys. **112**, 3090 (2000); J.B. Hooper, M.T. Pileggi, J.D. McCoy, J.G. Curro, and J.D. Weinhold, J.Chem. Phys. **112**, 3094 (2000); J. B. Hooper, J.D. McCoy, J.G. Curro, and F. van Swol, J. Chem. Phys. **113**, 2021 (2000).

24. A. Yethiraj and C. E. Woodward, J. Chem. Phys. **102**, 5499.

25. K. Huang and A. C. Balazs, Macromolecules **26**, 1914 (1993).

26. W. W. Graessley, R. C. Hayward, and G. S. Grest, Macromolecules, 32, 3510 (1999).

27. S. Mendez, J. G. Curro, M. Puetz, D. Bedrov, and G. D. Smith, J. Chem. Phys., **115**, 5669 (2001).

28. N.F. Carnahan and K. E. Starling, J. Chem. Phys. **51**, 635 (1969); D. J. Tildesley and W. B. Street, Mol. Phys. **41**, 341 (1980); J. Chang and S. I. Sandler, Chem.

Eng. Sci. **49** 2777 (1994); F. A. Escobedo and J. J. dePablo, J. Chem. Phys. **102**, 2636 (1995).

29. M. Aubouy, G.H. Fredrickson, P. Pincus, and E. Raphael, Macromolecules **28**, 2979 (1995).

Part 2: Effect of Inter-Molecular Attractions

Abstract

Density Functional Theory (DFT) was used to study polymer chains, tethered to a surface and in the presence of a solvent. For reasons of computational practicality, it is common practice to remove the explicit solvent molecules from the problem. Contact was made with two such models that we call the "implicit-solvent" and the "continuum-solvent" approximations. First, DFT was applied to tethered chains in an implicit-solvent. Using the equation-of-state of bead-spring chains as input, we found excellent agreement of the theory with density profiles obtained in the Molecular Dynamics simulations on the same model as a function of temperature. Next, DFT was applied to tethered chains in an incompressible, continuum-solvent. Using the Flory-Huggins theory as input, our DFT equations reduced to conventional self-consistent field theory. From our DFT formalism, we demonstrated that the implicit-solvent problem, at a given temperature, is equivalent to the continuum solvent problem, provided the chi parameter and total density are interpreted appropriately.

1. Introduction

Tethered polymer chains play an important role in the modulation of interactions between surfaces. A common example is Latex paint where strongly adsorbed chains are used as anti-flocculants; as two polymer-coated, ceramic surfaces approach each other, the tethered chains become entropically restricted and an effective repulsion is induced between the surfaces. Of course, if the solvent were a poor one, the polymer-solvent system's inclination to phase separate would result in an effective attraction between the surfaces in spite of the loss in conformational entropy and the particles would flocculate.

A closely related application is in pressure-sensitive adhesives. A bare surface is brought in contact with a polymer-coated surface, usually without solvent present. As before, there is a loss in conformational entropy but, in this case, whether the surfaces adhere or not depends upon the extent to which the polymer "wets" the bare surface. Here, the reduction in entropy competes against surface-tension effects while, in the flocculent case, it competes against mixing effects. Not surprisingly, the adhesive strength can be weakened by the presence of a small amount either of a good solvent for the polymer or of a solvent with a strong affinity for the surface.

These, then, are the two instances to bear in mind: tethered chains, first, in a relatively good solvent (a wet-brush) and, second, in a vacuum (a dry-brush). The quantity of interest in the current paper is the density profile of the chains near an isolated surface while the effective force between two surfaces will be addressed in a future publication.

Under normal conditions, the density profile of an isolated dry brush is relatively uninteresting: the polymer forms a constant density layer which drops off in a step-

function manner at a distance related to the chain length and surface coverage. This step-function density profile can be perturbed in two ways. First, if a second surface has been adhered to the chains, the density profile will develop more structural detail as the surfaces are pulled apart and the chains stretch in an effort to continue to wet the second surface. Second, if the chains are heated to sufficiently high temperature, they will attempt to vaporize and the density profile will elongate away from the wall. In order for the chains to be heated to the point where they extend from the wall requires temperatures that are unreasonably high for experimentally realizable polymers (i.e., temperatures that would rapidly degrade the polymer); however, computer simulations commonly probe this high temperature region.

The reason that the latter case of high-temperature, solvent-less brushes is of interest is that the high-temperature chain structures for these brushes are similar to the structures of room-temperature brushes in good solvents. In other words, the wet-brush case can be qualitatively studied with simulations of dry-brushes at high temperatures. This is illustrated in Fig. 1. The center schematic represents an experimentally realistic wet-brush while the right-hand schematic represents a high temperature dry-brush where the temperature has been tuned so that the chain distributions of the two cases are approximately the same. Such high-temperature, solvent-less brushes are often referred to as being in "continuum" solvents; however, since we will use this term for a different purpose, we refer to the high-temperature, solvent-less brush as being in an "*implicit*"-solvent. Moreover, for the remainder of the paper, we will reserve the term "dry-brush" for the low-temperature, step-function extreme of the implicit-solvent system.

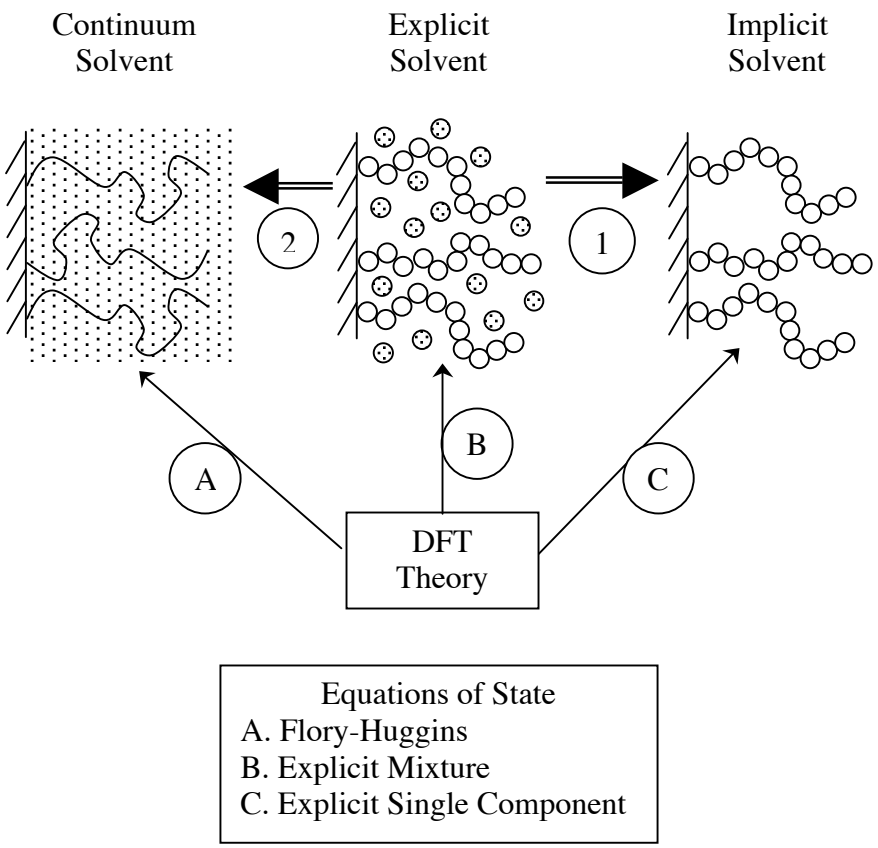

Figure 1: Mappings involved in the study of tethered chains. The center schematic represents wet brushes complete with explicit solvent molecules and realistic potential energy interactions between the sites. The right-most schematic represents the same polymer chains as in the center but lacking the solvent molecules. The left-most schematic represents thread-like chains in a continuum solvent with interactions dictated by a □-parameter and with incompressibility enforced. The circled numbers indicate various approximations discussed in the text. The circled letters indicate which equation of state is used in each case.

The usual mapping from the full wet-brush system with explicit-solvent to the implicit-solvent system is straightforward, and is denoted as mapping 1 in Fig. 1. Specifically, the radius of gyration, R_g, is found through computer simulation for a single chain in the implicit-solvent. The temperature where R_g varies as the chain length to the 1/2 power is identified as the theta-temperature, T_Θ, for the implicit-polymer "mixture". In the long chain limit, the theta temperature corresponds to a Flory-Huggins χ-parameter of 1/2. If χ is assumed to vary inversely with temperature, T, then χ for the implicit-solvent brush is approximately $T_\Theta/(2T)$. The physics of an explicit-solvent system is said to be well approximated by the implicit-solvent system if the χ's are the same for both – even if they are at different temperatures. That is,

$$\chi_{explicit} = \chi_{vacuum}$$

$$\left(\frac{T_\Theta}{2T}\right)_{explicit} = \left(\frac{T_\Theta}{2T}\right)_{vacuum} \qquad \text{(mapping 1)} \qquad (1.1)$$

where $T_{explicit} \neq T_{implicit}$ and $T_{\Theta,explicit} \neq T_{\Theta,implicit}$.

One expects this to be an approximate mapping for several reasons. First, experimental expressions for χ are usually of the form A+B/T (where A and B are constants) and not, simply, B/T. Second, the osmotic compressibility in the explicit solvent system is only roughly mimicked by the bulk compressibility in the implicit solvent case. And, finally, at the molecular level, the pair correlation functions in the explicit-solvent system are highly structured, while those in the implicit-solvent case are more gas-like.

Previously, tethered chains have been investigated from several different perspectives. Alexander[1] and de Gennes[2] used a scaling approach where the polymer profile was assumed to be a step function. More detailed predictions have been made by a

number of workers[3-8] who have adapted Self-Consistent Field (SCF) theory to the tethered chain problem. Under certain conditions, the SCF problem can be simplified and, as shown by Milner and collaborators[9], an analytic solution is found with a parabolic density profile. Finally, Carignano and Szleifer[10] developed the Single Chain Mean Field (SCMF) theory which treats the "single-chain" aspect of the problem more realistically than SCF theory does. The reader is referred to several reviews on tethered polymer chains that have appeared in the recent literature[11-13].

Density Functional Theory (DFT) is a powerful methodology for the modeling of inhomogeneous systems such as polymer brushes. In DFT theory, the molecules are treated as not interacting with each other, but, instead, an effective, medium-induced, external field is used to mimic the effect of the medium. There are two broad classes of polyatomic DFT theories: those focusing on the structure of the homogeneous liquid[14] and weighted-DFT theories that use the equation of state as the primary input.[15, 16] The former was applied to tethered polymer chains in an earlier work[17], referred to here as Paper I, in which a simplified version of DFT theory was developed and applied to "athermal" tethered chains both in implicit and in explicit solvents. The Paper I, DFT theory is of the hypernetted chain (HNC) form.

The inclusion of attractions into DFT theory can present special problems where the repulsions and attractions need be treated through different approximations as was found in the application of weighted-DFT theory to polymer liquids near surfaces.[18] In the current study, tethered chains with attractive interactions are investigated. Here, we also find that the attractive interactions between molecules require the use of a modified form of DFT theory in which a hybrid of HNC and Percus-Yevick (PY) DFT is

employed. In the appendix we show that the delta-function version of PY-DFT developed in this study is a special case of a more general DFT that results from a well-defined and physically motivated free energy functional. These various versions of DFT theory are contained in the "DFT theory" box in Fig. 1.

Tethered pearl-necklace chains in an implicit-solvent have been thoroughly studied with Molecular Dynamics computer simulations[19-25]. In the first part of the current paper, we use the results of these simulations as the basis for determining the degree of PY character needed by the DFT theory. The DFT theory uses the properties of the bulk system as "input", and, conveniently, the equation of state (EOS) for the bulk system has recently been accurately represented in analytic form[26]. This is EOS "C" in Fig. 1. Of course, if the results of simulations of explicit-solvent brushes were available, and if the EOS of the polymer / explicit-solvent mixture existed in analytic form (EOS "B" in Fig. 1), then a similar study of the explicit-solvent brush could be undertaken.

The explicit-solvent, wet-brush can be approximated in a second manner. This is mapping 2 in Fig. 1. Both the polymer and solvent interaction sites are reduced to point particles and the number of solvent molecules is increased so that the total density is constant through out the system. The resulting solvent is referred to as a "*continuum*" and the chains, as "*thread*"-like.

The continuum-solvent brushes can also be modeled by DFT theory. The HNC form of DFT theory for the mixture is used along with the (incompressible) Flory-Huggins description of the mixture (EOS "A" in Fig. 1). This results in a version of Self-Consistent Field (SCF) theory[3-8] (although, as discussed in Paper I, with finite "extensibility"). Neither attractive strength nor temperature enter SCF theory

independently: the only measure of attractive strength and temperature is the χ-parameter.

In the second part of the current paper we demonstrate that the implicit-solvent version of HNC/PY-DFT theory can be written in the form of the continuum-solvent version of HNC-DFT theory (i.e., SCF theory). Consequently, the χ-parameter that is central to SCF theory can be related to the bulk equation of state for the implicit-solvent case. The behavior we find for χ as a function of temperature is closer to the A+B/T form typical of explicit solvent systems. We suggest that this is a better way of relating the implicit-solvent to the explicit-solvent brushes than the previous $\chi=T_{\theta}/(2T)$ mapping.

It is useful to consider the information needed to uniquely determine the state of the three systems in Fig. 1. Tethered chains with explicit-solvent require a knowledge of the chain length, N; the solvent density, ρ_{sol}; the surface coverage, ρ_A; the temperature, T; the potential site-site energy function for polymer-polymer, $u_{PP}(\underline{r})$; for solvent-polymer, $u_{SP}(\underline{r})$; and for solvent-solvent, $u_{SS}(\underline{r})$. Tethered chains with implicit-solvent have the same N, ρ_A, and $u_{PP}(\underline{r})$ as the explicit-solvent case, but with a different T and no solvent. Tethered chains with continuum-solvent have the same N and ρ_A as the explicit-solvent case, but with a different ρ_{sol}; and the effect of temperature and potential energy functions are incorporated into a single χ-parameter.

In the remainder of the paper, we develop and expand upon the two issues mentioned above. First, we demonstrate that a highly simplified DFT theory can predict the structure of tethered chains in an implicit-solvent. Density profiles were calculated and compared to those found through Molecular Dynamics simulations[19-25]. Second, we

show that the implicit-solvent DFT theory can be mapped onto the continuum-solvent SCF theory[3-8] of tethered-chains.

2. Molecular Model and General Background

The model employed here has been well studied[19-26]. Neighboring sites are connected by a FENE bonding potential, and non-bonded sites interact through a Lennard-Jones 6-12 potential. For "thermal" chains the latter is

$$u(\underline{r}) = 4\left[\left(\frac{}{r}\right)^{12} - \left(\frac{}{r}\right)^{6}\right] \qquad (2.1)$$

and for "athermal" chains, is

$$u(\underline{r}) = 4\left[\left(\frac{}{r}\right)^{12} - \left(\frac{}{r}\right)^{6} + \frac{1}{4}\right] \qquad r \le 2^{1/6}$$
$$= 0 \qquad \text{otherwise} \qquad (2.2)$$

where (athermal)=1k_BT and k_B is the Boltzmann constant. Unless specifically indicated, all length are in units of , and all temperatures, in units of /k_B. Within the DFT theory, the bond lengths and site diameters were 1 . It should be noticed that although "athermal" is often taken to mean "the high temperature limit", the high temperature limit of u(r)/k_BT from Eq. (2.1) is zero and not the non-zero result of Eq. (2.2) with /k_BT =1. Consequently, one should not expect the DFT results of Eq. (2.1) to approach the athermal results in this limit.

Other miscellaneous "input" for DFT theory is also needed. The zero wavevector component of the direct correlation function, $\hat{c}(0)$, for the single component system is found from the equation of state and the thermodynamic relationship

$$\langle\rho\rangle\hat{c}(0) = \frac{1}{N}\rho - \frac{1}{\langle\rho\rangle k_B T \kappa_T} \tag{2.3}$$

where κ_T is the isothermal compressibility of the corresponding bulk polymer (same chain length and density). The number of sites in a chain is N, and $<\rho>$ is the mass-averaged polymer density given by

$$\langle\rho\rangle = \frac{\int_0^H \rho^2(z)dz}{\int_0^H \rho_1(z)dz} \tag{2.4}$$

with H being the distance between the walls and $\rho(z)$, the inhomogeneous site density of the tethered chains. The equation of state for athermal, hard-site chains is taken from a Carnahan-Starling-like curve fit[27] of simulation results, and, for thermal tangent site chains, from the more complex, 33-parameter curve fit by MacDowell et al.[26].

Although the DFT theory is applicable to tethered chains in the dilute, mushroom regime, we have applied the theory only to more concentrated systems where there is some degree of chain overlap and a one-dimensional density profile can be assumed. That is, we restrict our attention to surface coverages, Γ_A, greater than

$$\Gamma_A^* = \frac{1}{\pi R_g^2} = \frac{6}{\pi\sigma^2} N^{-2\nu} \tag{2.5}$$

where R_g is the radius of gyration, $R_g \approx \sigma N^{\nu}/\sqrt{6}$, and ν is the Flory exponent. Once the chains begin to overlap, the local density experienced by a site is given by the bulk solution average at the dilute to semi-dilute crossover:

$$\rho^* \sim \frac{3N}{4\pi Rg^3} \sim \frac{3.5}{\pi^3 N^{3\nu}\sigma^3} \tag{2.6}$$

As long as $\rho_A > \rho_A^*$, we expect our assumption of a one-dimensional field and profile to be valid. However, as discussed in Paper I, it is possible that the average density calculated from Eqn. (2.4) is less than ρ^* while $\rho_A > \rho_A^*$. When this occurs, we take our average density, $<\rho>$, to be ρ^*. In this lower cut-off, we take $\rho^*=[\rho^*(\sigma=1/2)+ \rho^*(\sigma=3/5)]/2$. Consequently, $\rho^*\sigma^3$ is 0.32 for N=50; 0.22 for N=100; and 0.15 for N=200. Of course, as the chains become longer, ρ^* decreases in both magnitude and computational importance.

The HNC form of the effective external fields $U_p^0(z)$ and $U_s^0(z)$ from Paper I are

$$\begin{aligned} U_p^0(z) &= U_p(z) - \hat{c}_{pp}(0)\rho_p(z) - \hat{c}_{ps}(0)\rho_s(z) + \lambda(z) \\ U_s^0(z) &= U_s(z) - \hat{c}_{sp}(0)\rho_p(z) - \hat{c}_{ss}(0)\rho_s(z) + \lambda(z) \end{aligned} \tag{2.7}$$

where constant terms have been dropped. The bare external fields are $U_p(z)$ and $U_s(z)$. The polymer is denoted by the subscript "p" and the solvent, by "s". For the implicit-solvent case, subscripts are dropped since only "p"-terms are present. The undetermined multiplier, $\lambda(z)$, is used to enforce incompressibility and is set to zero for compressible systems.

3. Density Functional Theory for Implicit-Solvents

Density Functional Theory can be viewed as the solution of two coupled, functional equations

$$\begin{aligned} \rho(z) &= F[U^0(z)] \\ U^0(z) &= G[\rho(z)] \end{aligned} \tag{3.1}$$

where F[…] is a functional which transforms an arbitrary external field, $U^0(z)$, into the density profile of a melt of ideal chains in the presence of that field. In the simplest case of single, un-tethered sites, the F-functional is simply the Boltzmann function: $\rho(z) = \rho_0 \exp\left(-\beta U^0(z)\right)$ where ρ_0 is a normalization constant. For tethered chains, F[…] is more complex, but the density, $\rho(z)$, can be computed numerically using Fourier Transforms: details were reported in Paper I.

The G-functional is less mathematically complex; however, much of its simplicity is the result of its approximate nature. The HNC form of the effective external field for an implicit-solvent is

$$U^0(z) = U(z) - \hat{c}(0)\rho(z) \tag{3.2}$$

which is a special case of Eqn. (2.7). In the spirit of SCF theory, the direct correlation function was approximated as having only a delta-function range. For cases where there is an attractive component to the site-site interactions, this delta-function approximation causes the polymers to "wet" the wall in cases where it should de-wet. To correct this, we split the direct correlation function into a repulsive and an attractive contribution. The repulsive contribution to the direct correlation function, $\hat{c}^R(0)$, comes from the hard site equation of state as in Paper I, and the attractive, $\hat{c}^A(0)$, from $\hat{c}^A(0) = \hat{c}(0) - \hat{c}^R(0)$. The HNC form of the external field becomes

$$U^0(z) = U(z) - \hat{c}^R(0)\rho(z) - \hat{c}^A(0)\tilde{\rho}(z) \qquad \text{(HNC)} \tag{3.3}$$

where $\tilde{\rho}(z)$ is the density averaged over the range of the interaction potential and has the effect of reintroducing non-locality into field. This introduces a length scale into the direct correlation function. Previous work[28] has demonstrated that the detailed form of

the direct correlation function is not crucial so long as its range and integrated area are fixed. If we assume that $c^A(|\underline{r}|)$ is constant over the range $0 \le |\underline{r}| \le a$, then $\tilde{\rho}(z)$ has the simple form

$$\tilde{\rho}(z) = \frac{3}{4a^3} \int_{-a}^{a} \rho(z+r)\left(a^2 - r^2\right) dr \qquad (3.4)$$

where, unless otherwise noted, the range of the attractions, "a", is taken to be 1Å. Similar approaches to the averaging of the density for the attractions have been used in the DFT context for polymer melts[18].

The HNC form of the field is less accurate[28,29] for high density, repulsive interactions than that of the Percus-Yevick (PY) form:

$$U^0(z) = U(z) - \ln\left[1 + \hat{c}^R(0)\delta\rho(z)\right] - \hat{c}^A(0)\tilde{\rho}(z) \qquad \text{(PY)} \qquad (3.5)$$

where $\delta\rho(z)=\rho(z)-\langle\rho\rangle$. In this, the delta-function limit, the PY-field results from a well-defined and physically motivated free energy expansion; however, in the case of more realistic c(r)'s, the PY-form does not result in a natural manner from a free energy functional. Instead, as shown in the appendix, such a generalization to non-local c(r)'s, suggests a modified PY-form.

Since when $\hat{c}^R(0)\delta\rho(z) \sim 0$, the PY form is identical to that of the HNC, the two forms are most distinct when $\hat{c}^R(0)$ is large in magnitude. A mixture of 60% of the HNC form with 40% of the PY form was empirically found to result in the best overall accuracy. Unless otherwise indicated, this mixing was used in the calculations reported here.

It is useful to think in terms of the effective external "force": $f(z)=-dU^0(z)/d\rho(z)$ where a positive force would tend to increase the density at a given z, and a negative

force, to decrease it. For the HNC field, the total force, $\hat{c}^R(0)+\hat{c}^A(0)$, is independent of the local density, and, since for strong attractions, $\hat{c}^A(0)\sim-\hat{c}^R(0)$, the total effective force of the HNC field is nearly zero *for all ρ(z).* On the other hand, the force for the PY form of the field is $\hat{c}^R(0)/\left[1+\hat{c}^R(0)\rho(z)\right]+\hat{c}^A(0)$. Now, as seen in Fig. 2, even for strong attractions, the force displays positive regions where the density is enhanced, and negative regions where the density is strongly depressed. In particular, at the high

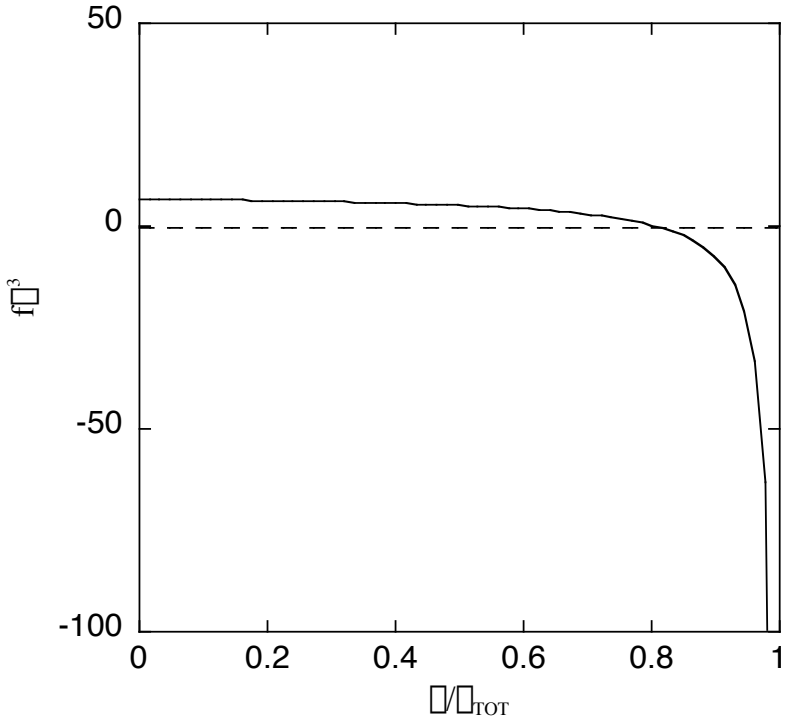

Figure 2: The force on the site density, $f=-dU^0/d\rho$, for (N=50, $\sigma_A^2=0.1$, $k_BT/\varepsilon=2$) chains vs. site density for the HNC (dashed) and PY (solid) fields. The parameters for the 60% HNC/40%PY solution were used: $\langle\rho\sigma^3\rangle=0.511$, $\rho_{tot}\sigma^3=0.624$, $\hat{c}^R(0)=-8.85\sigma^3$ and $\hat{c}^A(0)=8.30\sigma^3$.

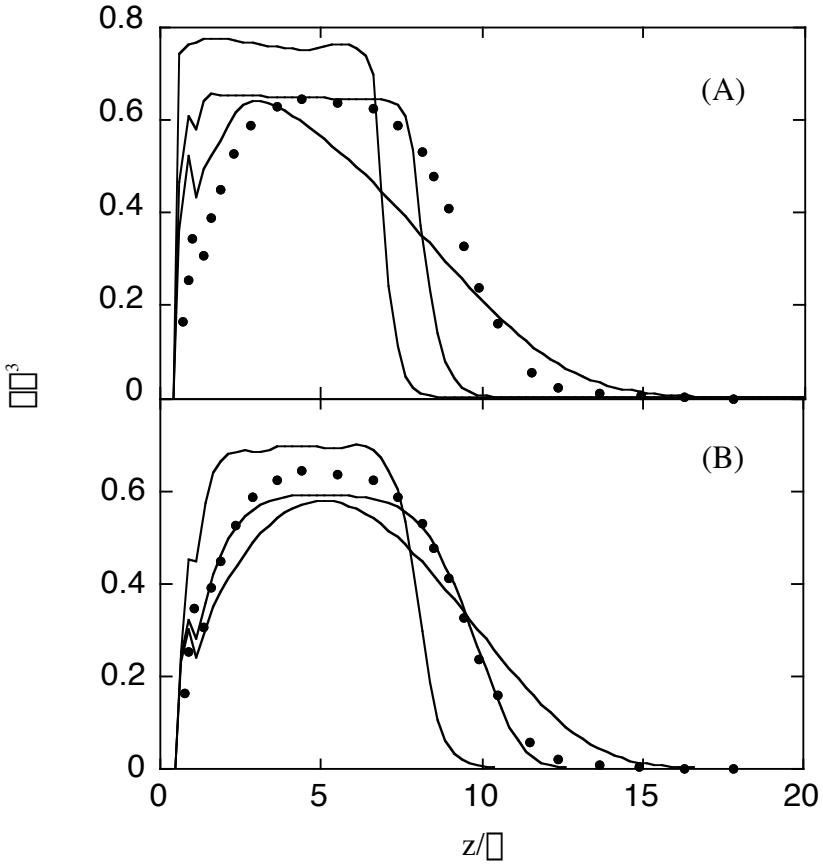

Figure 3: Density profiles of (N=50, $\sigma_A\sigma^2$=0.1, k_BT/ε=2) chains. The dots are the simulation results of Grest et al.[21]. The solid lines, from least to most extended, are the results of DFT theory for pure PY; for 60% HNC/40%PY; and for pure HNC. In (A), the range of the density average in $\tilde{\rho}(z)$ is zero (a=0), and, in (B), the range is one (a=1). In (B), the "mixture" parameters for the 60/40 case are $\rho_{tot}\sigma^3$=0.624, $\rho_\infty^{\varepsilon}$=2.59, ρ_∞^{R}=-0.946, and ρ_∞=1.64.

density of $\rho(z) = \left(\hat{c}^R(0)\langle\rho\rangle + 1\right)/\hat{c}^R(0)$, the force becomes negative infinity and, consequently, $\rho(z)$ must be less than $\rho_{tot} = \left(\hat{c}^R(0)\langle\rho\rangle + 1\right)/\hat{c}^R(0)$ at all z.

In Fig. 3a, the HNC; the 60%HNC/40% PY; and PY cases are shown for 50 site chains at a temperature of 2 and a surface coverage of 0.1. Here the attractive

contribution has a cutoff a=0 in the average of Eqn. (3.4). Both the PY and 60%HNC/40% PY fields have strong step function characters; however, all three fields yield density profiles that are too strongly weighted towards the wall. By setting the range of the average to a=1 (that is, introducing a non-local character to the field), the density profile is pulled away from the wall as seen in Fig. 3b.

The mechanics of the iterative solution are, roughly, as follows. The density profile is guessed to be a constant between the walls and zero otherwise. The field is calculated from this density profile, and a new density profile is calculated from the field. The initial density profile is mixed with the new profile to yield an input density, and the loop begun again. The process is repeated until no point in the "new" density profile differs from the "input" profile by more than a maximum "test" value (usually set at ~1%). The mixing of the density profiles has 1 to 5% of the "new" density. The distance between the walls is divided into bins of width 0.25Å. The evaluation of the "F"-functional requires between 300 and 600 Fourier components, and between 100 and 400 Picard iterations are needed for convergence.

4. Results for Implicit-Solvents

We have compared the density profile results of DFT theory to a wide range of simulation results. The only large "adjustment" of the theory was in the choice of the ratio of HNC to PY character (60%HNC) in the field. Other "smaller" adjustments – such as the range and shape of the direct correlation function – were selected to be as simple as was reasonable. Again, the primary feature that is captured by the new version of DFT theory is the step-like nature of the density profile at large surface coverages, large chain lengths, and low temperatures.

In the next few figures, the ability of the 60/40 DFT theory to reproduce simulation results is demonstrated. Density profiles for N=50, athermal chains are shown in Fig. 4a and the DFT theory is seen to be of a quality similar to the HNC-DFT theory of Paper I. In Fig. 4b, the effect of temperature on N=50 chains is explored, and the DFT theory captures the chain collapse to a high degree of accuracy. In Fig. 5, the densities of N=100 chains are displayed for a variety of surface coverages and temperatures, and the agreement between DFT theory and simulation is excellent for all cases. In Fig. 6a, the densities for N=200, $\rho_A\sigma^2$=0.03 are compared: the theory predicts a slightly stronger condensation on the wall than seen in the simulation, but, over all, DFT theory works well. Finally, in Fig. 6b, the densities for N=200, $\rho_A\sigma^2$=0.1 are shown – for both simulation and DFT theory - and are seen to develop a very pronounced step behavior at low temperature.

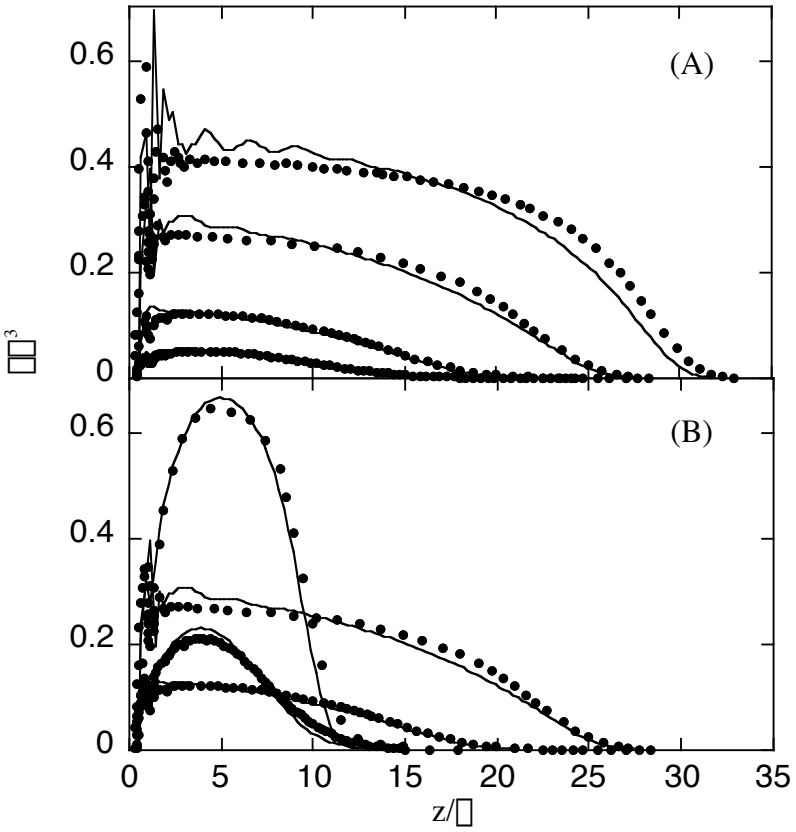

Figure 4: Density profiles for N =50 chains. In (A), the chains are athermal and σ_A^2 is, from low to high peak values, 0.01,0.03,0.1,0.2. In (B), from lowest to highest peak value the results are for (σ_A^2=0.03,athermal), (σ_A^2=0.03,T=3), (σ_A^2=0.1,athermal), (σ_A^2=0.1,T=2). The symbols are the results of the simulations of Murat et al.[20]; the lines, of 60%HNC/40%PY DFT theory.

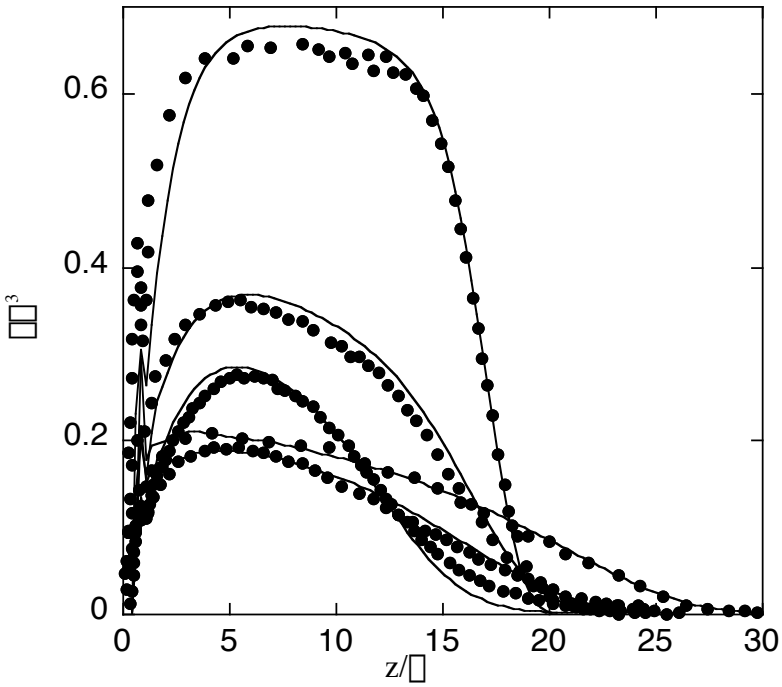

Figure 5: Density profiles for N=100 chains, from lowest to highest peak values: ($\varepsilon_A\sigma^2$=0.027,T=4), ($\varepsilon_A\sigma^2$=0.036,T=5), ($\varepsilon_A\sigma^2$=0.03,T=3), ($\varepsilon_A\sigma^2$=0.05,T=3), ($\varepsilon_A\sigma^2$=0.1,T=2). The symbols are the results of the simulations of Grest et al.[21,24], the $\varepsilon_A\sigma^2$=0.027 and 0.036 cases have small but non-zero wall attractions; the lines are the results of 60%HNC/40%PY DFT theory.

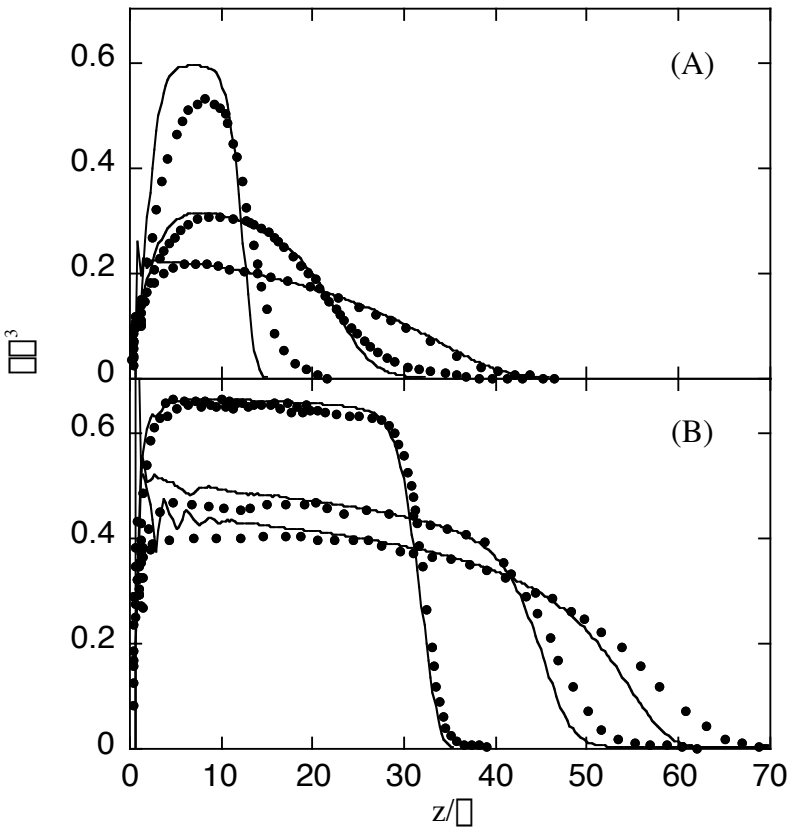

Figure 6: Density profiles for N=200 chains. In (A), $\rho_A\sigma^2$=0.03, and in (B), $\rho_A\sigma^2$=0.1. In both cases, the temperatures from lowest to highest peak values are: 4, 3, 2. The symbols are the results of the simulations of Grest et al.[21]; the lines, of 60%HNC/40%PY DFT theory.

5. Mapping of the Implicit onto the Continuum-Solvent

In section 3 we considered the implicit-solvent which permitted us to make detailed comparisons with the results of Molecular Dynamics simulations. Now, we turn our attention to the continuum-solvent, which will permit us to make contact with SCF theory. It will then be seen that the two different solvent-types can be mapped one onto the other.

The development of the implicit-solvent DFT theory begins with the general HNC-DFT equation for a mixture and with the direct correlation functions evaluated from the Flory-Huggins theory[30] of mixtures:

$$A_{Mix} = V\frac{\rho_P}{N}\ln(\rho_P) + \rho_S\ln(\rho_S) + \rho_S\rho_P\chi_A \tag{5.1}$$

where A_{Mix} is the Helmholtz Free Energy of mixing on a constant volume, V, lattice. The volume fraction of the polymer, ρ_P, is $\rho_P/(\rho_P+\rho_S)$ and the solvent volume fraction is defined in an analogous manner where "S" denotes "solvent" and "P", "polymer". In the zero wavevector limit, the inverse structure factors, $\hat{S}^{-1}_{\alpha,\beta}(0)$, are related to thermodynamic derivatives of Eqn. (5.1):

$$\hat{S}^{-1}_{\alpha,\beta}(0) = \frac{1}{k_B TV}\left(\frac{\partial^2 A_{Mix}}{\partial\rho_\alpha\,\partial\rho_\beta}\right)_{T,V} \tag{5.2}$$

which are in turn related[31] to the direct correlation functions:

$$\begin{aligned}\hat{C}_{PP}(0) - \hat{C}_{PS}(0) &= \frac{1}{N\rho_P}\left[\hat{S}^{-1}_{PP}(0) + \hat{S}^{-1}_{PS}(0)\right]\\ \hat{C}_{PS}(0) - \hat{C}_{SS}(0) &= -\frac{1}{N\rho_P}\left[\hat{S}^{-1}_{PS}(0) + \hat{S}^{-1}_{SS}(0)\right]\end{aligned}. \tag{5.3}$$

This results in

$$\hat{C}_{PP}(0) - \hat{C}_{PS}(0) = -\frac{1}{\rho_P+\rho_S}\left[1 - \frac{1}{N} - 2\chi^A\rho_S\right]$$
$$\hat{C}_{PS}(0) - \hat{C}_{SS}(0) = -\frac{1}{\rho_P+\rho_S}\left[1 - \frac{1}{N} + 2\chi^A\rho_P\right]. \qquad (5.4)$$

As a result, the HNC field for the incompressible mixture of Eqn. (2.7) becomes

$$U_P^0(z) = U_P(z) + \left[1 - \frac{1}{N} - 2\chi^A(1 - \langle\rho_P\rangle)\right](\rho_P(z) - \langle\rho_P\rangle) + \xi(z)$$
$$U_S^0(z) = U_S(z) + \left[1 - \frac{1}{N} + 2\chi^A\langle\rho_P\rangle\right](\rho_P(z) - \langle\rho_P\rangle) + \xi(z) \qquad (5.5)$$

where $\langle\rho_P\rangle$ is the average polymer density divided by the total density, ρ_{tot}. The undetermined multiplier, $\xi(z)$, enforces $\rho_{tot}=\rho_P(z)+\rho_S(z)$. Since $\xi(z)$ is a function which is only defined so that this constraint is true, it can be replaced with $\xi'(z) = \xi(z) + f(z)$ where f(z) is any function of z. As a result of this manipulation, the fields can be written as

$$U_P^0(z) = U_P(z) - \chi^A\rho_P(z) + \xi'(z)$$
$$U_S^0(z) = U_S(z) + \chi^A\rho_P(z) + \xi'(z) \qquad (5.6)$$

which is the form most often employed in SCF theory[3-8]. This permits us to connect the SCF and DFT theories.

Moreover, if the undetermined multiplier in Eqn. (5.6) is eliminated, then a mapping is seen between the continuum and implicit-solvent systems. In particular, since the F functional can be written analytically for the solvent species: $\rho_S(z) = \rho_{tot}\exp\left(-U_S^0(z)\right)$, the second equation in Eqn. (5.6) can be used to eliminate $\xi'(z)$. The resulting polymer field is

$$U_P^0(z) = U_P(z) - U_S(z) - 2\chi^A\rho_P(z) - \ln(1 - \rho_P(z)). \qquad (5.7)$$

(Incidentally, this is a reformulation of SCF theory without the use of undetermined multipliers.)

Now let us compare the continuum-solvent field (Eqn. (5.7)) with the one for implicit-solvents (Eqn. (3.5)). It can be seen that the SCF field becomes the "implicit-solvent" PY field if the following substitutions are made

$$\begin{aligned} \rho_{tot} &\rightarrow \frac{\hat{C}^R(0)\langle\rho\rangle - 1}{\hat{C}^R(0)} \\ \frac{2\pi^A}{\rho_{tot}} &\rightarrow \hat{C}^A(0) \end{aligned}, \tag{5.8}$$

and if a constant, which does not influence the density profile, is dropped. Of course, since both $\langle\rho\rangle$ and the $\hat{C}(0)$'s are self-consistently linked to the density profile, "ρ_{tot}" and "π^A" will depend on surface coverage, chain length and temperature in a complex manner.

The 60%HNC/40%PY form of DFT theory used here can be written as

$$U_P^0(z) = U_P(z) - U_S(z) - 2\left(\pi^A + \pi^R\right)\rho_P(z) - \ln\left(1 - \rho_P(z)\right) \tag{5.9}$$

where the entropic π^R is a function of volume fraction

$$2\pi^R = -\left[\rho_{tot}\hat{C}^R(0) + \frac{\ln\left(1-\rho_P(z)\right)}{\rho_P(z)}\right] \tag{5.10}$$

where α=0 for pure PY; α=1 for pure HNC; and, in our work, α=0.6. In order to explore the temperature dependence of $\pi=\pi^A+\pi^R$, the large z limit of π, π_∞, is taken to give

$$\pi = \pi_\bullet + \frac{\rho}{2}\left[1 + \frac{\ln\left(1-\rho_P(z)\right)}{\rho_P(z)}\right]. \tag{5.11}$$

For the 60%HNC/40%PY case in Fig. 3b, this yields $\rho_{tot}\sigma^3$=0.624, π_∞^A=2.59, π_∞^R=-0.946, and π_∞=1.64 for these quantities.

6. Results for the Continuum-Solvent

As discussed above, a "melt" of tethered chains (defined by N, ϕ_A, and T) can be viewed as a polymer solution (defined by N, ϕ_A, ϕ_{tot}, and χ). Consequently, every density profile generated by DFT can also be predicted by SCF theory *with the correct choice of parameters*. Clearly, the relationships between the SCF parameters (N, ϕ_A, ϕ_{tot}, χ) and the DFT parameters (N, ϕ_A, and T) are non-trivial. Indeed, an arbitrary selection of SCF parameters may be inconsistent with the behavior of the system at any N, ϕ_A, and T.

From the calculations for the implicit-solvent that resulted in Figs. 3b – 6, the value of χ_∞ that would apply to the continuum-solvent can be extracted. This quantity is plotted as a function of 1/T in Fig. 7. The functional form of χ_∞ is seen to be roughly as expected from Flory-Huggins theory. Specifically, χ_∞ varies inversely with temperature, but with a non-zero intercept due to the repulsive (or entropic) contribution of χ^R. The χ-temperature for isolated chains of this system is roughly 3 as found in a number of studies: Grest and Murat[21] reported 3.0±0.1; Weinhold and Kumar[25], 3.0; Harismiadis and Szleifer[32], 3.9; and Kumar[33], 2.75. Consequently, the χ in the continuum-solvent interpretation of the DFT treatment of the tethered chains should be roughly 0.5 at a temperature of approximately 3 – as it is.

Tracking the average extension of the chain, or layer thickness, as defined by $Z_{avg} = \int_0^{H/2} z\phi(z)dz \Big/ \int_0^{H/2} \phi(z)dz$ can be used to monitor the formation of the dense layer of polymer on the surface. As seen in Fig. 8, Z_{avg} decreases slowly with temperature at high temperature; rapidly at intermediate temperature; and is a constant at low temperature. The temperature where the chain extension starts to drop rapidly can be quantified by

drawing straight lines for the high temperature and intermediate temperature results. The location of this "knee" in the behavior is plotted as a function of chain length in Fig. 9. In the insert to Fig. 9, it is seen that the "transition" temperature varies roughly as the chain length to the 0.28 power. Also plotted are the liquid-gas critical points for chains of varying lengths.

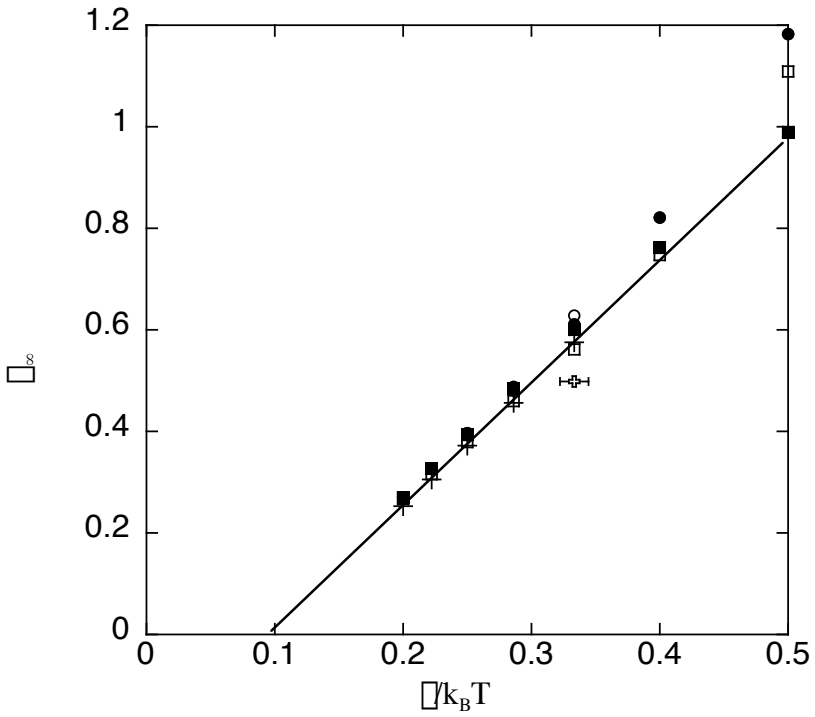

Figure 7: The $\Box_\infty$ parameter in the polymer solution interpretation of the DFT theory. The filled circles denote ($\Box_A\Box^2$=0.1,N=50); the filled squares, ($\Box_A\Box^2$=0.03,N=50); the open circles, ($\Box_A\Box^2$=0.1,N=100); the open squares, ($\Box_A\Box^2$=0.03,N=100); the solid crosses, ($\Box_A\Box^2$=0.03,N=200). The Maltese cross denotes the $\Box$-point predict from the bulk simulations of Grest et al.[21]. The line which roughly fits the data is $2.4\Box/k_BT - 0.23$.

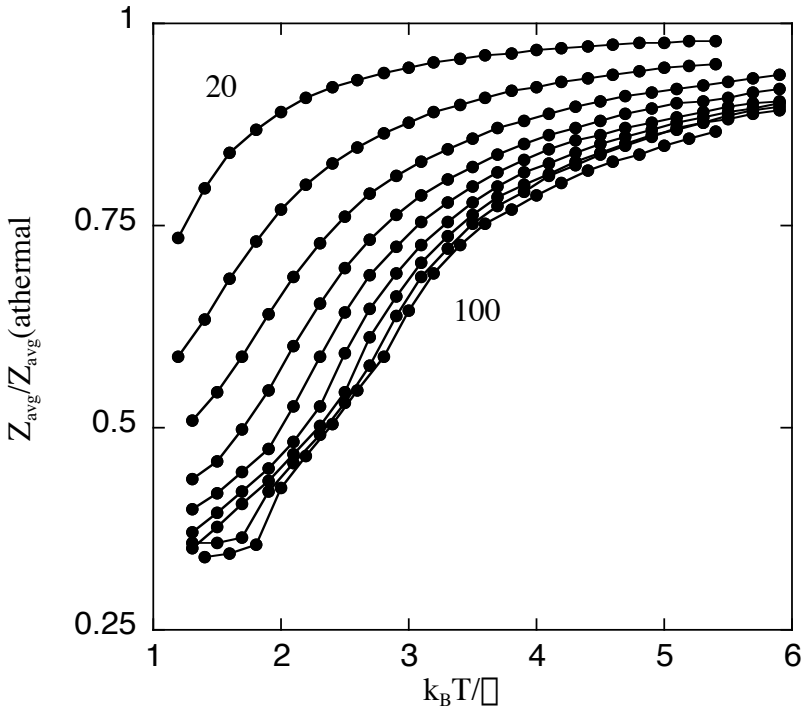

Figure 8: The average extension of the chains relative to the extension of athermal chains. Results are presented for chain lengths N=20, 30, 40, 50, 60, 70, 80, 90, and 100 with larger chain lengths corresponding to smaller relative extensions. In all cases, $\epsilon_A\epsilon^2 = 0.03$.

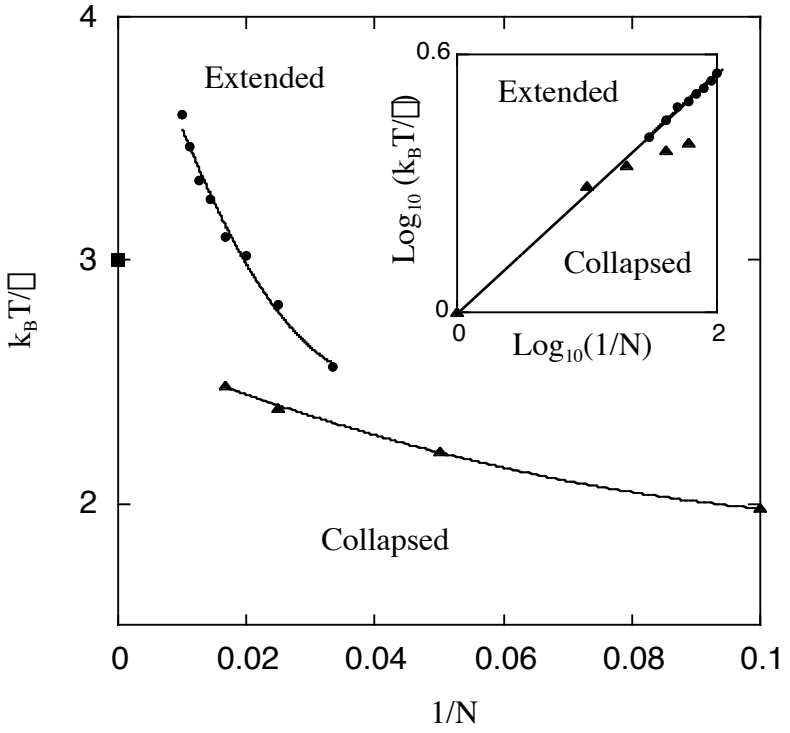

Figure 9: The "transition" between extended and collapsed. The circles denote the temperature at the "knee" of the curves in Fig. 8. The triangles are critical temperatures for polymer melts[26], and the square is the "Θ-temperature" for chains of infinite length[21].

7. Conclusions

In the current paper, the connection between the DFT and SCF theories was further elucidated. In order to do so, DFT theory was expressed in its simplest form that was consistent with computer simulations of tethered chains. In the first phase of this effort (Paper I), it was found that an HNC form of the DFT equations with all coefficients taken to be "local" in nature worked very well for athermal chains. On the other hand,

chains with attractions demand a modification of the form of the equations with the repulsive contribution to the DFT equations having a degree of PY character.

When this was done, the coarse features of simulations of tethered chain profiles were reproduced. At high temperature the chains extended from the surface while at low temperature, the chains formed an (essentially) constant density layer. In order to capture the detailed nature of the low temperature profiles, a non-local nature was added to the attractive contribution to the density. This was done by averaging the density used in the attractive field term over a radius of □- an approach similar to that used for inhomogeneous melts[18]. As a result and in keeping with simulation, the polymer sites tended to "de-wet" from the wall in order to maximize their number of neighbors. Considering the simplicity of the theory, the simulation results were predicted extremely well.

While the ability to model tethered chains with DFT theory was a satisfying outcome, the most interesting aspect of our work was the furthering of our understanding of the relationship between the (continuum-solvent) SCF and (implicit-solvent) DFT theories. By writing (single-component) DFT theory in the same form as (binary-mixture) SCF theory, it was shown that the pure PY form of the DFT theory is identical to SCF theory except that ρ_{tot} and □ of the mixture are dictated by the single-component polymer equation-of-state rather than being free parameters. In the form of the DFT theory that best describes the tethered chain behavior (60%HNC/40%PY), the □ parameter turned out to have a volume-fraction dependence. The □ far from the wall, ρ_{∞}, was found to be roughly linear with inverse temperature in keeping with Flory-Huggins

theory but with a non-zero intercept. Moreover, Γ_∞ was found to be insensitive to surface coverage and to converge quickly with chain length.

Finally, we demonstrated that as the temperature is decreased, the chains go through a region of rapid collapse analogous to the liquid-gas transition in a bulk polymer. Through the mapping of the "implicit" polymer brush onto the mixture of polymer / continuum-solvent, we predict a similar transition in the wet polymer brush.

Appendix: Incompressible Density Functional Theory

An important aspect of the inter-relationship between the implicit and the continuum solvent treatment of tethered chains is the route that it suggests for the development of a new density functional – a functional we refer to as Ye-McCoy-Curro Density Functional Theory (YMC-DFT). The field resulting from the minimization of the YMC-DFT has a strong Percus-Yevick flavor, however, there has been no previous treatment at the free energy functional level.

For the purposes of this development, we drop the implicit solvent notation and treat an inhomogeneous polymer with only a single site type, although the generalization to different site types and to mixtures is straightforward. The Hypernetted Chain (HNC) approximation to the Grand Potential free energy[34] is

$$\begin{aligned} \Delta W = \Delta W_p^0 &+ \int \Delta\Omega_p^0(\underline{r})\Delta\rho_p(\underline{r})d\underline{r} - \int \Delta\Omega_p(\underline{r})\Delta\rho_p(\underline{r})d\underline{r} \\ &- \frac{k_B T}{2}\iint c_{pp}(\underline{r}-\underline{r}')\Delta\rho_p(\underline{r})\Delta\rho_p(\underline{r}')d\underline{r}d\underline{r}' \end{aligned} \tag{A.1}$$

where W=-PV = -(pressure)(volume). The superscript "0" denotes the ideal system; and the difference "Δ", the inhomogeneous minus the homogeneous state (for instance,

$\Delta\rho_p(\underline{r}) = \rho_p(\underline{r}) - \rho_{p,h}$ where "h" denotes the homogeneous state). The subscript "p" denotes "polymer" and $c_{pp}(\underline{r})$ is the direct correlation function. The generalized field is $\omega(\underline{r})=\mu-U(\underline{r})$ where μ is the chemical potential and $U(\underline{r})$ is the external field. The ideal Grand Potential functional is

$$W_p^0 = k_B T \int \cdots \int \exp\left[\sum_{i=1}^{N} \omega_p^0(\underline{r}_i)\right] S(\underline{r}_1,\cdots,\underline{r}_N)\, d\underline{r}_1,\cdots,d\underline{r}_N \qquad (A.2)$$

where the summation is over the sites on the polymer and the function S contains the bonding constraints (a product of displaced delta functions for the freely jointed chain).

This functional is then minimized with respect to the density under the constraint

$$\rho_p(\underline{r}) = \int \cdots \int \frac{1}{N} \sum_{j=1}^{N} \delta(\underline{r}_j - \underline{r}) \exp\left[\sum_{i=1}^{N} \omega_p^0(\underline{r}_i)\right] S(\underline{r}_1,\cdots,\underline{r}_N)\, d\underline{r}_1,\cdots,d\underline{r}_N . \qquad (A.3)$$

Minimizing the free energy with respect to both the density and the ideal field enforces this constraint. As long as the free energy is in the form given in Eq. (A.1), the undetermined multiplier is zero – resulting in a notational simplification. The condition $\frac{\delta W}{\delta \omega_p^0(\underline{r})} = 0$ results in Eqn. (A.3) while $\frac{\delta W}{\delta \rho_p(\underline{r})} = 0$ results in the HNC-field

$$\omega_p^0(\underline{r}) = \omega_p(\underline{r}) + k_B T \int c_{pp}(\underline{r} - \underline{r}')\, \Delta\rho_p(\underline{r}')\, d\underline{r}' \qquad (A.4)$$

which, to within a constant becomes Eqn. (3.2) when the direct correlation function is approximated as a delta function.

Undetermined multipliers are useful for enforcing an equality such as in Eqn. (A.3); however, enforcing an inequality such as $\rho(r)\le\rho_{tot}$ requires other methods. One such method relies upon the introduction of a second species whose only role is to enforce this inequality. In particular, let us imagine that there is a background,

incompressible “solvent” in the problem in the spirit of the continuum-solvent discussed above where

$$\rho_{tot} = \rho_p(\underline{r}) + \rho_s(\underline{r}) \tag{A.5}$$

at all $\underline{r}$ in both inhomogeneous and homogeneous cases where ρ_{tot} is the “total density” and “s” denotes “solvent”. The mixture generalization of Eqn. (A.1) is

$$\begin{aligned}\beta W = \beta W_p^0 &+ \int \rho_p^0(\underline{r})\, V_p(\underline{r})\, d\underline{r} - \int \rho_p(\underline{r})\, V_p(\underline{r})\, d\underline{r} \\ &+ \beta W_s^0 + \int \rho_s^0(\underline{r})\, V_s(\underline{r})\, d\underline{r} - \int \rho_s(\underline{r})\, V_s(\underline{r})\, d\underline{r} \\ &- \frac{k_B T}{2} \sum_{i,j=p,s} \iint c_{i,j}(\underline{r} - \underline{r}')\, \Delta\rho_i(\underline{r})\, \Delta\rho_j(\underline{r}')\, d\underline{r} d\underline{r}'\end{aligned} \tag{A.6}$$

Before minimizing this functional, notice that for an atomic solvent, the constraint (A.3) can be inverted to give

$$V_s^0(\underline{r}) = k_B T \ln(\rho_s(\underline{r})) \tag{A.7}$$

Substituting Eqn. (A.5) and (A.7) into the free energy (A.6) yields

$$\begin{aligned}\beta W = \beta W_p^0 &+ \int \rho_p^0(\underline{r})\, V_p(\underline{r})\, d\underline{r} - \int \rho_p(\underline{r})\, V_p(\underline{r})\, d\underline{r} \\ &+ k_B T \int \Delta\rho_p(\underline{r})\, d\underline{r} + k_B T \int \left(\rho_{s,h} - \Delta\rho_p(\underline{r})\right) \ln\left(\frac{\rho_{s,h} - \Delta\rho_p(\underline{r})}{\rho_{s,h}}\right) d\underline{r} \\ &- \frac{k_B T}{2} \iint \left[c_{pp}(\underline{r} - \underline{r}') - 2c_{sp}(\underline{r} - \underline{r}') + c_{ss}(\underline{r} - \underline{r}')\right] \Delta\rho_p(\underline{r})\, \Delta\rho_p(\underline{r}')\, d\underline{r} d\underline{r}'\end{aligned} \tag{A.8}$$

The minimization of (A.8) with respect to $\rho_p^0(\underline{r})$ still results in Eqn. (A.3) while the minimization with respect to $\rho_p(\underline{r})$ yields

$$\begin{aligned}\Delta V_p^0(\underline{r}) = \Delta V_p(\underline{r}) &+ k_B T \ln\left(1 - \frac{\Delta\rho_p(\underline{r})}{\rho_{s,h}}\right) \\ &+ k_B T \int \left[c_{pp}(\underline{r} - \underline{r}') - 2c_{sp}(\underline{r} - \underline{r}') + c_{ss}(\underline{r} - \underline{r}')\right] \Delta\rho_p(\underline{r}')\, d\underline{r}'\end{aligned} \tag{A.9}$$

To this point, we have not specified the properties of the "solvent" other than that it "fills-up" the density to ρ_{tot} at all $\underline{r}$. This fictitious "solvent" can be expected to limit the range of $\rho_p(\underline{r})$ to be less than ρ_{tot}; however, in order to be consistent, the YMC-field (A.9) should agree with the HNC-field (A.4) for small $\Delta\rho_p(\underline{r})$. Consequently,

$$2c_{sp}(\underline{r}) - c_{ss}(\underline{r}) = -\frac{\Delta(\underline{r})}{\rho_{s,h}} \tag{A.10}$$

and the density of the solvent in the homogeneous system, $\rho_{s,h}$, can then be used to "tune" the potential. A reasonable choice is to split the contributions to the field between attractive and repulsive contributions. This can be done by choosing $\rho_{s,h} = -1/\hat{c}^R_{pp}(0)$ where $\hat{c}^R_{pp}(0)$ is the integrated value of the direct correlation function of the polymer melt with only repulsive interactions. The YMC-field then becomes

$$\begin{aligned}\Delta\Delta^0_p(\underline{r}) = {} & \Delta\Delta_p(\underline{r}) + k_BT\ln\left[1+\hat{c}^R_{pp}(0)\Delta\rho_p(\underline{r})\right] \\ & + k_BT\int\left[c_{pp}(\underline{r}-\underline{r}') - \hat{c}^R_{pp}(0)\delta(\underline{r}-\underline{r}')\right]\Delta\rho_p(\underline{r}')d\underline{r}'\end{aligned}. \tag{A.11}$$

More concisely, this can be written as

$$\Delta\Delta^0_p(\underline{r}) = \Delta\Delta_p(\underline{r}) + k_BT\ln\left[1+\hat{c}^R_{pp}(0)\Delta\rho_p(\underline{r})\right] + k_BT\hat{c}^A_{pp}(0)\Delta\tilde{\rho}_p(\underline{r}) \tag{A.12}$$

where

$$\hat{c}^A_{pp}(0) = \int\left[c_{pp}(\underline{r})\right]d\underline{r} - \hat{c}^R_{pp}(0) \tag{A.13}$$

and

$$\tilde{\rho}_p(\underline{r}) = \frac{\int\left[c_{pp}(\underline{r}-\underline{r}') - \hat{c}^R_{pp}(0)\delta(\underline{r}-\underline{r}')\right]\rho_p(\underline{r}')d\underline{r}'}{\hat{c}^A_{pp}(0)}. \tag{A.14}$$

To within an additive constant, Eqn. (A.12) is Eqn. (3.5).

Once minimized, the field can be substituted into Eqn. (A.8) to give

$$\beta W = k_B T \left(\rho_{p,h} - \frac{1}{\hat{c}^R_{pp}(0)} \right) \int \ln\left[1 + \hat{c}^R_{pp}(0)\,\delta\rho_p(\underline{r})\right] d\underline{r} + \frac{k_B T}{2} \iint \left[c_{pp}(\underline{r}-\underline{r}') - \hat{c}^R_{pp}(0)\,\delta(\underline{r}-\underline{r}')\right] \delta\rho_p(\underline{r}) \left[\delta\rho_p(\underline{r}') + \rho_{p,h}\right] d\underline{r}\, d\underline{r}' \quad . \tag{A.15}$$

In addition to tuning the field through the selection of $\rho_{s,h}$, the average between the HNC and YMC Functionals can be taken as

$$\beta W = \alpha\, \beta W_{HNC} + (1-\alpha)\, \beta W_{YMC} \tag{A.16}$$

where βW_{YMC} is the functional of Eqn. (A.8) and βW_{HNC}, of Eqn. (A.1). In the current study, we found that α=0.60 worked well.

An interesting generalization is to use an averaged polymer density in the density constraint: $\rho_{tot} = \bar{\rho}_p(\underline{r}) + \rho_s(\underline{r})$ where $\bar{\rho}_p(\underline{r}) = \int \omega(\underline{r}-\underline{r}')\rho_p(\underline{r}')\, d\underline{r}'$ and $\omega(\underline{r})$ is a normalized weighting function. Following the minimization procedure outlined above, the full YMC-DFT field becomes

$$\beta\omega^0_p(\underline{r}) = \beta\omega_p(\underline{r}) + k_B T \int \omega(\underline{r}-\underline{r}') \ln\left[1 + \hat{c}^R_{pp}(0)\,\delta\bar{\rho}_p(\underline{r}')\right] d\underline{r}' + k_B T \int \left[c_{pp}(\underline{r}-\underline{r}') - c^R_{pp}(\underline{r}-\underline{r}')\right] \delta\rho_p(\underline{r}')\, d\underline{r}' \tag{A.17}$$

where, in Fourier space, the weighting function is

$$\left[\hat{\omega}(k)\right]^2 = \frac{\hat{c}_{pp}(k)}{\hat{c}_{pp}(0)} \quad . \tag{A.18}$$

In the delta-function limit, the YMC-field becomes identical to the PY-field; however, for other cases, the YMC-field has different physics. The degree to which the YMC-theory differs from PY will depend upon the application. On the other hand, the YMC approach results from the minimization of a free energy while the PY has a corresponding free energy only in the case of direct correlation functions that are delta functions.

References

1. S. Alexander, J. Phys. (Paris) **38**, 983 (1977).
2. P. G. de Gennes, Macromolecules **13**, 1069 (1980).
3. J. M. H. M. Scheutjens and G. J. Fleer, J. Phys. Chem. **83**, 1619 (1979).
4. T. Cosgrove, T. Heath, B. van Lent; and J. M. H. M. Scheutjens, Macromolecules **20**, 1692 (1987).
5. K.R. Shull, J. Chem. Phys. **94**, 5723 (1991).
6. R. Baranowski and M. D. Whitmore, J. Chem. Phys. **108**, 9885 (1998).
7. M. Laradji, H. Guo, and M. J. Zuckermann, Phys. Rev. E **49**, 3199 (1994).
8. J.I. Martin and Z.G. Wang, J. Phys. Chem. **99**, 2833 (1995).
9. S.T. Milner, J. Chem. Soc. Faraday Trans. **86** 1349 (1990); S. T. Miller, T. A. Witten, and M. E. Cates, **21**, 2610 (1988).
10. M. A. Carignano and I. Szleifer, J. Chem. Phys. **98**, 5006 (1993);
11. I. Szleifer and M. A. Carignano, Adv. Chem. Phys. **94**, 165 (1995); I. Szleifer and M. A. Carignano, Macromol. Rapid Commun. **21**, 423 (2000).
12. S. T. Milner, Science **251**, 905 (1991).
13. A. Halperin, M. Tirrell, and T.P. Lodge, Adv. Polym Sci. **100**, 31, (1991).
14. D. Chandler, J. D. McCoy, and S. J. Singer, J. Chem. Phys. **85**, 5971 (1986).
15. E. Kierlik and M.L. Rosinberg, J. Chem. Phys. **100**, 1716 (1994).
16. C.E. Woodward, J. Chem. Phys. **97**, 4525 (1992);
    A. Yethiraj and C.E. Woodward, J. Chem. Phys. **102**, 5499 (1995).
17. J. D. McCoy, Y. Ye, and J. G. Curro, J. Chem. Phys. **117**, 2975 (2002).
18. C.N. Patra, A. Yethiraj, J. Chem. Phys. **111**, 1608 (1999);

C.N. Patra, A. Yethiraj, J. Chem. Phys. **112**, 1579 (2000);

M. Muller, L.G. MacDowell, A. Yethiraj, J. Chem. Phys. **118**, 2929 (2003).

19. G. S. Grest and M. Murat, in *Monte Carlo and Molecular Dynamics Simulations in Polymer Science*, ed. K. Binder (Oxford Univ. Press, NY, 1995), p 476.
20. M. Murat and G. S. Grest, Macromolecules **22**, 4054 (1989).
21. G. S. Grest and M. Murat, Macromolecules **26**, 3108 (1993).
22. G. S. Grest, J. Chem. Phys. **105**, 5532 (1996).
23. M. Murat and G. S. Grest, Phys. Rev. Lett. **63**, 1074 (1989); G.S. Grest, Private Communication.
24. G.S. Grest, Macrommolecules **27**, 418 (1994).
25. J.D. Weinhold and S.K. Kumar, J. Chem. Phys. **101** 4312 (1994).
26. L. MacDowell, M. Mueller, C. Vega and K. Binder, J. Chem. Phys., **113**, 419 (2000). Notice that the indices i and j in Table IV of this paper are reversed, Private Communication.
27. J.D. McCoy, M.A. Teixeira, and J.D. Curro, J. Chem, Phys. **114**, 4289 (2001).
28. J.B. Hooper, J.D. McCoy, and J.G. Curro, J. Chem. Phys. **112**, 3090 (2000); J.B. Hooper, M.T. Pileggi, J.D. McCoy, J.G. Curro, and J.D. Weinhold, J.Chem. Phys. **112**, 3094 (2000); J. B. Hooper, J.D. McCoy, J.G. Curro, and F. van Swol, J. Chem. Phys. **113**, 2021 (2000).
29. J. P. Donley, J. G. Curro, and J. D. McCoy, J. Chem. Phys. **101**, 3205 (1994).
30. P.J. Flory, *Principles of Polymer Chemistry*, Cornell University Press, Ithaca, NY, 1953.

31. J.G. Kirkwood and F.P. Buff, J. Chem. Phys. **19**, 774 (1951).

32. V. I. Harismiadis and I. Szleifer Mol. Phys. **81** 851 (1994).

33. S.K. Kumar, J. Chem. Phys. **96**, 1490 (1992).

34. See appendices of J.D. McCoy, K.G. Honnell, K.S. Schweizer, and J.G. Curro, J. Chem. Phys. **95**, 9348 (1991) and references cited there in.

Distribution:

6	MS 1349	John G. Curro, 01834
3	MS 1349	John D. McCoy, NM Tech
1	MS 0102	Joan B. Woodard, 00002
1	MS 1411	Eliot Fang, 01834
1	MS 1411	Amalie L. Frischknecht, 01834
1	MS 1411	David R. Heine, 01834
1	MS 1411	Mark J. Stevens, 01834
1	MS 1415	Gary S. Grest, 01114
1	MS 9108	Central Technical Files, 08945-1
2	MS 0899	Technical Library, 09616
1	MS 0323	LDRD Office, 01011